JOURNAL OF GUIDANCE, CONTROL, AND DYNAMICS
Vol. 27, No. 5, September–October 2004

# Integrated Power and Attitude Control with Spacecraft Flywheels and Control Moment Gyroscopes

Carlos M. Roithmayr*
*NASA Langley Research Center, Hampton, Virginia 23681-2199*
and
Christopher D. Karlgaard,† Renjith R. Kumar,‡ and David M. Bose§
*Analytical Mechanics Associates, Inc., Hampton, Virginia 23666*

**A law is designed for simultaneous control of the orientation of an Earth-pointing spacecraft, the energy stored by counter-rotating flywheels, and the angular momentum of the flywheels and control moment gyroscopes used together as an integrated set of actuators for attitude control. General, nonlinear equations of motion are presented in vector-dyadic form and used to obtain approximate expressions that are then linearized in preparation for design of control laws that include feedback of flywheel kinetic energy error as a means of compensating for damping exerted by rotor bearings. Two flywheel steering laws are developed such that torque commanded by an attitude control law is applied while energy is stored or discharged at the required rate. With use of the International Space Station as an example, numerical simulations are performed to demonstrate control about a torque equilibrium attitude and to illustrate the benefits of kinetic energy error feedback.**

## Introduction

FLYWHEELS offer great promise for reducing the mass and extending the life of spacecraft; they store more energy per unit of mass and last significantly longer than chemical batteries. Moreover, flywheels can simultaneously store energy and exert torque on a spacecraft, which makes it possible for one system of flywheels to replace two separate systems typically used for energy storage and attitude control. When the mass of the two conventional systems is taken into account, the specific energy of flywheel systems is expected to be 5–10 times greater, according to Christopher and Beach.[1] The attitude control system typically represents 11% of the mass of a spacecraft, and batteries make up 6% of the mass; replacing 17% of a spacecraft's mass with a flywheel system whose mass is 1.7% would lead to a 15% reduction in total spacecraft mass. Secondary benefits occur as well. Because flywheels have higher system level efficiencies than batteries, a reduction in solar array size and mass becomes possible, and reboost propellant can be reduced because the smaller arrays produce less drag. Flywheel systems are expected to last 15 years (Ref. 1) or more, whereas typical batteries last only 5 years. The greatest advantage of flywheels over batteries accrues in low Earth orbit, where eclipse happens more frequently and for larger fractions of an orbit than in higher orbits. Repeated charge and discharge cycles and high depth of discharge significantly degrade batteries over time.

In the mid-1980s designers considered the use of flywheels on the space station as discussed, for example, in Refs. 2 and 3. More recently, there were plans[4] to replace the International Space Station (ISS) batteries with a flywheel energy storage system (FESS); hence, there naturally arose the thought of using the flywheels to assist the ISS double-gimbaled control moment gyroscopes (CMGs) in controlling attitude. A numerical investigation of the merits of this idea requires a feedback control law designed for CMGs and flywheels used together as an integrated set of effectors. The current CMG control law described in Refs. 5 and 6 seeks a time-varying torque equilibrium attitude (TEA) for the vehicle by minimizing a cost function involving spacecraft attitude and angular speed and CMG angular momentum. A CMG steering law, such as the one developed by Kennel in Ref. 7, determines the speeds of the two gimbals (in which each constant speed CMG rotor is mounted) needed to produce the torque requested by the control law. As a natural extension of the present approach, we seek a new control law derived from a cost function that includes flywheel angular momentum in addition to the aforementioned quantities. Also needed is a "flywheel steering law," a counterpart to the CMG steering law that will determine the motor-generator torque to be applied to each member of a counter-rotating flywheel pair such that rotational kinetic energy is stored or discharged in the required manner and that the net torque requested by the control law is produced simultaneously.

A review of the literature does not reveal any existing three-axis TEA-seeking control laws for Earth-pointing spacecraft using flywheels and CMGs together, or even flywheels alone, where attitude control, momentum management, and power management are addressed in a unified way. In Ref. 8, Notti et al. give a sketch of a control law and an energy distribution law; however, this work is not applicable primarily because each flywheel rotor is assumed to be supported by two gimbals and the ISS FESS did not contain any gimbals. In addition, the control law lacks flywheel angular momentum as a feedback parameter. The authors of Ref. 9 examine the use of two double-gimbaled flywheels, operated as a single scissored pair, to provide energy storage and control the attitude of an inertially oriented spacecraft subject to constant disturbance torque. Simulations involving hardware in the loop, and numerical models of the hardware, show that such a flywheel configuration can meet stringent inertial pointing requirements. The recent work on control laws for integrated power and attitude control systems reported in Refs. 10–12 deals with sets of four or more flywheels whose spin axes are noncollinear and is, therefore, not directly applicable to the counter-rotating flywheel pair arrangement of the FESS. Other current research, described in Refs. 13–15, is concerned with sets of variable-speed, single-gimbal control moment gyroscopes. Varatharajoo and Fasoulas develop control laws in Ref. 16 for a

Presented as Paper 03-124 at the AAS/AIAA Space Flight Mechanics Meeting, Ponce, Puerto Rico, 9 February 2003; received 23 April 2003; revision received 16 December 2003; accepted for publication 23 January 2004. 

*Aerospace Engineer, Spacecraft and Sensors Branch, Mail Stop 328; c.m.roithmayr@larc.nasa.gov. Senior Member AIAA.

†Project Engineer, 303 Butler Farm Road, Suite 104 A; karlgaard@ama-inc.com. Member AIAA.

‡President, 303 Butler Farm Road, Suite 104 A; renji@ama-inc.com. Member AIAA.

§Supervising Engineer, 303 Butler Farm Road, Suite 104 A; dmbose@ama-inc.com.

spacecraft using a counter-rotating flywheel configuration; however, they only consider a pitch-axis controller.

Hall's control law, proposed in Ref. 10, is an open-loop scheme (rather than a feedback law) for performing large-angle attitude maneuvers. It does not account for gravitational and aerodynamic torques that have a significant effect on the motion of ISS and, therefore, can not be used for maintaining TEA, the primary job of the CMGs. Hall introduces a flywheel steering law based on a matrix pseudoinverse; it is applied in each of Refs. 11–15. Tsiotras et al.[11] employ Lyapunov stability theory to develop a feedback control law that performs well in simulations involving disturbance torques; however, flywheel momentum is managed by expenditure of propellant. Costic et al. develop in Ref. 12 a nonlinear controller that includes an adaptive scheme for estimating the mass distribution of the spacecraft, but they do not address momentum management.

In Ref. 13, Fausz and Richie extend the work of Hall[10] to a nonlinear feedback controller applicable to a set of variable-speed, single-gimbal control moment gyroscopes. The discussion is continued in Ref. 14, and simulation results are presented, but momentum management is not addressed in either Ref. 13 or 14. Yoon and Tsiotras develop an adaptive nonlinear control law in Ref. 15 and incorporate wheel-speed equalization to reduce the possibility of singularities and to keep the wheel speeds within acceptable limits. Numerical simulation results show that attitude and power profiles can be tracked even when the spacecraft inertia properties are unknown. Of all of references the mentioned heretofore, Ref. 15 is the only one in which attitude control, momentum management, and power management for flywheels is considered in an integrated fashion.

Note that Refs. 10–16 fail to take into account damping torque exerted by the spacecraft and a flywheel rotor on each other; in practice, this will cause the actual rotational kinetic energy possessed by the flywheels to differ from the required amount. None of these works include any feedback of errors in flywheel speed, power, or kinetic energy, something that must be done under realistic conditions.

Numerical simulation results are presented in Ref. 17 for a laboratory apparatus consisting of two counter-rotating flywheels mounted on an air-bearing platform that is free to rotate about a single vertical axis. The simulations demonstrate behavior of a direct current (dc) bus regulation algorithm and a single-axis proportional–integral–derivative (PID) attitude control law operating simultaneously in three situations: a constant commanded platform angle during transitions through charge, charge reduction, and discharge modes; step responses during flywheel discharge to changes in commanded angle; and step responses during flywheel discharge to changes in disturbance torque, respectively. An algorithm for dc bus regulation and experimental results are reported in Refs. 18 and 19.

In what follows we present equations of motion to be used in numerical simulations and in control law design, develop an algorithm for managing momentum and maintaining torque equilibrium attitude, construct two flywheel steering laws, and present simulation results showing the performance of the control law as well as the benefits of flywheel kinetic energy error feedback.

## Equations of Motion for Spacecraft with Flywheels and CMGs

### Dynamical Equations

The system of interest $S$ is composed of a rigid body $B$ moving in an inertial or Newtonian reference frame $N$ and several rigid axisymmetric rotors $R_1, \ldots, R_\rho$ whose mass centers are fixed in $B$. A subset of the rotors $R_1, \ldots, R_\mathcal{F}$ have spin axes fixed in $B$ so that these rotors represent nongimbaled flywheels or reaction wheels. Each of the remaining rotors $R_{\mathcal{F}+1}, \ldots, R_\rho$ are attached to $B$ with one or more massless gimbals that permit the direction of the spin axis to change relative to $B$; these rotors, thus, represent a number of CMGs, $\mathcal{C} = \rho - \mathcal{F}$. (The latter subset could contain variable speed flywheel rotors mounted in one or two gimbals, as well as constant speed CMGs, but we concern ourselves in this work only with nongimbaled flywheels.) This system is shown in Fig. 1, with rotors $R_2, \ldots, R_{\rho-1}$ omitted for the sake of clarity.

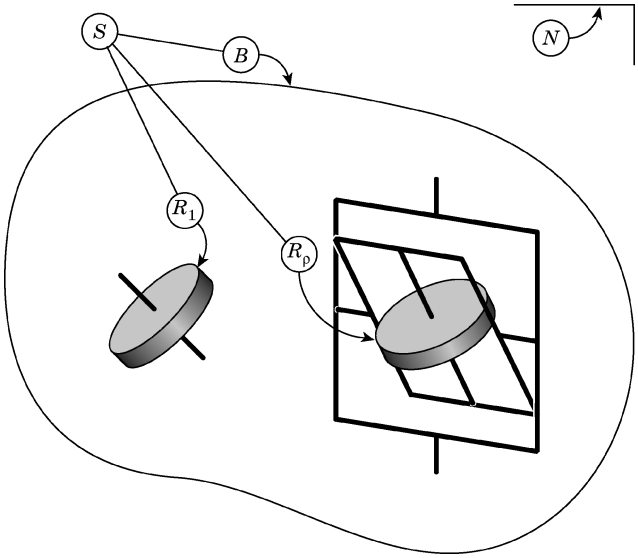


**Fig. 1 Spacecraft with flywheel and CMG.**

The equations of motion are derived using Kane's method [Eqs. (6.1.2), Ref. 20]

$$K_r + K_r^* = 0, \qquad r = 1, \ldots, n \tag{1}$$

where $K_r$ are generalized active forces for $S$ in $N$, $K_r^*$ are generalized inertia forces for $S$ in $N$, and $n$ is the number of degrees of freedom of $S$ in $N$.

The system $S$ is holonomic, and therefore, a complete description of the motion of $S$ in $N$ requires $n$ generalized speeds $u_1, \ldots, u_n$, conveniently chosen as follows:

$$^N\boldsymbol{\omega}^B = u_1\hat{\boldsymbol{b}}_1 + u_2\hat{\boldsymbol{b}}_2 + u_3\hat{\boldsymbol{b}}_3 \tag{2}$$

where $^N\boldsymbol{\omega}^B$ is the angular velocity of $B$ in $N$ and $\hat{\boldsymbol{b}}_1$, $\hat{\boldsymbol{b}}_2$, and $\hat{\boldsymbol{b}}_3$ are a set of mutually orthogonal, right-handed unit vectors fixed in $B$.

We introduce unit vectors $\hat{\boldsymbol{\beta}}_i$ fixed in $B$ such that they are each parallel to the spin axis of a flywheel rotor $R_i$ and, therefore, to the angular velocity $^B\boldsymbol{\omega}^{R_i}$ of $R_i$ in $B$. Generalized speeds $u_4, \ldots, u_{\mathcal{F}+3}$ associated with the flywheels can then be used to write the angular velocities as

$$^B\boldsymbol{\omega}^{R_i} = \begin{cases} u_{2i+2}\hat{\boldsymbol{\beta}}_i, & i = 1, \ldots, \mathcal{F}/2 \\ u_{2i-3}\hat{\boldsymbol{\beta}}_i, & i = \mathcal{F}/2+1, \ldots, \mathcal{F} \end{cases} \tag{3}$$

where we assume an even number of flywheel rotors $\mathcal{F}$ arranged in counter-rotating pairs.

The inner gimbal of each CMG is fastened to $B$ with a revolute joint in a single-gimbal configuration, whereas a double-gimbal CMG has the inner gimbal attached with a revolute joint to an outer gimbal, which is in turn mounted in $B$ with a second revolute joint. The axis of each revolute joint is assumed to pass through the mass center of the rotor, which is, thus, fixed in $B$. To maintain generality with regard to the number of CMG rotors and gimbals, the angular velocities $^B\boldsymbol{\omega}^{R_{\mathcal{F}+1}}, \ldots, ^B\boldsymbol{\omega}^{R_\rho}$ of the rotors relative to $B$ are not written explicitly, but they must be functions of the generalized speeds $u_{\mathcal{F}+4}, \ldots, u_{n-3}$, where one generalized speed is required for every gimbal.

The final three generalized speeds are associated with the velocity of the mass center $S^*$ of $S$ in $N$,

$$^N\boldsymbol{v}^{S^*} = u_{n-2}\hat{\boldsymbol{n}}_1 + u_{n-1}\hat{\boldsymbol{n}}_2 + u_n\hat{\boldsymbol{n}}_3 \tag{4}$$

where $\hat{\boldsymbol{n}}_1$, $\hat{\boldsymbol{n}}_2$, and $\hat{\boldsymbol{n}}_3$ are a set of mutually orthogonal, right-handed unit vectors fixed in $N$.

Let $\sigma$ be the set of external forces exerted on $S$. The forces in $\sigma$ acting on $B, R_1, \ldots, R_\rho$ are equivalent to single forces $\boldsymbol{F}_B, \boldsymbol{F}_1, \ldots, \boldsymbol{F}_\rho$ applied at the mass centers $B^*, R_1^*, \ldots, R_\rho^*$ of bodies $B, R_1, \ldots, R_\rho$, respectively, together with couples whose torques are $\boldsymbol{M}_B, \boldsymbol{M}_1, \ldots, \boldsymbol{M}_\rho$.

To account for the internal forces exerted by $B$ on $R_i$, we regard them as equivalent to a single force $\boldsymbol{F}^{B/R_i}$ applied at $R_i^*$, together

with a couple whose torque is $\boldsymbol{M}_T^{B/R_i}$. Because $R_i^*$ is fixed in $B$, $\boldsymbol{F}^{B/R_i}$ contributes nothing to $K_r$, $i = 1, \ldots, \rho$ and $r = 1, \ldots, n$, as discussed in Sec. 4.5 of Ref. 20.

The generalized active forces for $S$ in $N$ are obtained by application of Eq. (4.6.1) of Ref. 20 and are given by

$$K_r = {}^N\boldsymbol{v}_r^{S^*} \cdot \boldsymbol{F} + {}^N\boldsymbol{\omega}_r^B \cdot \boldsymbol{M} + \sum_{i=1}^{\rho} {}^B\boldsymbol{\omega}_r^{R_i} \cdot \left(\boldsymbol{M}_i + \boldsymbol{M}_T^{B/R_i}\right)$$

$$r = 1, \ldots, n \quad (5)$$

where ${}^N\boldsymbol{v}_r^{S^*}$ is known as the $r$th partial velocity of $S^*$ in $N$, ${}^N\boldsymbol{\omega}_r^B$ is the $r$th partial angular velocity of $B$ in $N$, and so forth. The vector $\boldsymbol{F}$ is the resultant of the forces in $\sigma$ acting on $S$,

$$\boldsymbol{F} = \boldsymbol{F}_B + \sum_{i=1}^{\rho} \boldsymbol{F}_i$$

and $\boldsymbol{M}$ is the moment of $\sigma$ about $S^*$, given by

$$\boldsymbol{M} = \boldsymbol{M}_B + \boldsymbol{r}^{S^*B^*} \times \boldsymbol{F}_B + \sum_{i=1}^{\rho} \left(\boldsymbol{M}_i + \boldsymbol{r}^{S^*R_i^*} \times \boldsymbol{F}_i\right)$$

where $\boldsymbol{r}^{S^*B^*}$ is the position vector from $S^*$ to $B^*$, etc.

The generalized inertia forces for $S$ in $N$ are formed according to Eqs. (4.11.5–4.11.7) of Ref. 20 and are given by

$$K_r^* = -{}^N\boldsymbol{v}_r^{S^*} \cdot m_S {}^N\boldsymbol{a}^{S^*} - {}^N\boldsymbol{\omega}_r^B \cdot \left[ \underline{\boldsymbol{I}}^{S/S^*} \cdot {}^N\boldsymbol{\alpha}^B + {}^N\boldsymbol{\omega}^B \times \underline{\boldsymbol{I}}^{S/S^*} \cdot {}^N\boldsymbol{\omega}^B \right.$$
$$+ \sum_{i=1}^{\rho} \left( \frac{{}^B\mathrm{d}}{\mathrm{d}t} {}^B\boldsymbol{H}^{R_i/R_i^*} + {}^N\boldsymbol{\omega}^B \times {}^B\boldsymbol{H}^{R_i/R_i^*} \right)$$
$$\left. + \sum_{i=\mathcal{F}+1}^{\rho} \left( {}^B\boldsymbol{\omega}^{R_i} \times \underline{\boldsymbol{I}}^{R_i/R_i^*} - \underline{\boldsymbol{I}}^{R_i/R_i^*} \times {}^B\boldsymbol{\omega}^{R_i} \right) \cdot {}^N\boldsymbol{\omega}^B \right]$$
$$- \sum_{i=1}^{\rho} {}^B\boldsymbol{\omega}_r^{R_i} \cdot \frac{{}^N\mathrm{d}}{\mathrm{d}t} {}^N\boldsymbol{H}^{R_i/R_i^*} \qquad r = 1, \ldots, n \quad (6)$$

where $m_S$ is the mass of system $S$, ${}^N\boldsymbol{a}^{S^*}$ is the acceleration of $S^*$ in $N$, $\underline{\boldsymbol{I}}^{S/S^*}$ is the inertia dyadic of $S$ for $S^*$, ${}^N\boldsymbol{\alpha}^B$ is the angular acceleration of $B$ in $N$, $\underline{\boldsymbol{I}}^{R_i/R_i^*}$ is the inertia dyadic of $R_i$ for $R_i^*$, and ${}^B\boldsymbol{H}^{R_i/R_i^*}$ and ${}^N\boldsymbol{H}^{R_i/R_i^*}$ are the central angular momenta of $R_i$ in $B$ and in $N$, respectively. Differentiation with respect to time in $B$ and in $N$ are indicated by ${}^B\mathrm{d}/\mathrm{d}t$ and ${}^N\mathrm{d}/\mathrm{d}t$, respectively.

According to Eqs. (1), the generalized inertia forces from Eqs. (6) are added to the generalized active forces from Eqs. (5) to yield vector-dyadic equations of motion for a spacecraft containing flywheels and CMGs,

$${}^N\boldsymbol{v}_r^{S^*} \cdot \left(\boldsymbol{F} - m_S {}^N\boldsymbol{a}^{S^*}\right)$$
$$+ {}^N\boldsymbol{\omega}_r^B \cdot \left\{ \boldsymbol{M} - \left[ \underline{\boldsymbol{I}}^{S/S^*} \cdot {}^N\boldsymbol{\alpha}^B + {}^N\boldsymbol{\omega}^B \times \underline{\boldsymbol{I}}^{S/S^*} \cdot {}^N\boldsymbol{\omega}^B \right.\right.$$
$$+ \sum_{i=1}^{\rho} \left( \frac{{}^B\mathrm{d}}{\mathrm{d}t} {}^B\boldsymbol{H}^{R_i/R_i^*} + {}^N\boldsymbol{\omega}^B \times {}^B\boldsymbol{H}^{R_i/R_i^*} \right)$$
$$\left.\left. + \sum_{i=\mathcal{F}+1}^{\rho} \left( {}^B\boldsymbol{\omega}^{R_i} \times \underline{\boldsymbol{I}}^{R_i/R_i^*} - \underline{\boldsymbol{I}}^{R_i/R_i^*} \times {}^B\boldsymbol{\omega}^{R_i} \right) \cdot {}^N\boldsymbol{\omega}^B \right] \right\}$$
$$+ \sum_{i=1}^{\rho} {}^B\boldsymbol{\omega}_r^{R_i} \cdot \left( \boldsymbol{M}_i + \boldsymbol{M}_T^{B/R_i} - \frac{{}^N\mathrm{d}}{\mathrm{d}t} {}^N\boldsymbol{H}^{R_i/R_i^*} \right) = 0$$

$$r = 1, \ldots, n \quad (7)$$

Equations (7) are completely general with regard to the number and orientation of flywheel rotors and the number of CMG rotors and gimbals. In this form, they are applicable to variable-speed CMGs. These equations of motion, and the expression for generalized inertia forces, can be compared briefly to previous work.

Reference 21 is concerned with gyrostats and relevant equations that can be dealt with easily by an analyst and quickly by a computer. Expressions for generalized inertia forces are presented separately for a gyrostat containing a single cylindrical rotor and for one containing a single spherical rotor; an underlying general relationship (C65) developed in Appendix C in Ref. 21 can be shown to give rise to Eqs. (6) presented here, when no CMGs are present ($\mathcal{C} = 0$, thus, $\rho = \mathcal{F}$). The term in the second line of Eqs. (C65) accounts for but a single rotor, although additional rotors can be handled straightforwardly by adding a sum of similar terms. The correspondence between Eqs. (C65) (Ref. 21) and our Eq. (6) is shown by appealing to Eqs. (24), (C61), (C35), (C24), (3), and (C34) of Ref. 21 and replacing their labels $G$, $B$, and $A$ for the gyrostat, rotor, and carrier, respectively with our $S$, $R_i$, and $B$. The use of the system mass and inertia scalars, together with the moment of inertia for the axis of symmetry of each rotor, is shown in Ref. 21 to lead to greater efficiency than use of mass properties of individual bodies in a gyrostat; this advantage happens to accrue to Eqs. (6) and (7) developed here.

Rheinfurth and Carroll present vector-dyadic equations of motion (27) (in Ref. 22) for a spacecraft composed of a rigid carrier and a rigid appendage whose mass center is fixed in the carrier. Additional appendages are accounted for easily by forming a sum, as they do in Eq. (16) (Ref. 22), but the resulting vector-dyadic expression will give rise to only three scalar equations. It is pointed out near the bottom of p. 6 (Ref. 22) that a CMG can be regarded as an appendage; however, the motion of every appendage relative to the carrier must be prescribed if the three relationships are to serve as dynamical equations governing the motion of the carrier. Reference 22 does not contain counterparts to the $n - 6$ of our Eqs. (7) that govern the motion of the rotors, or to the three equations governing the translational motion of the system. It can be shown rather easily that Rheinfurth and Carroll's Eqs. (27) give way to the first three of Eqs. (7) here when all rotors are permitted to be CMGs ($\mathcal{F} = 0$, thus, $\rho = \mathcal{C}$). After forming the required sum, and replacing their symbols $\underline{\mathrm{L}}$ with $\boldsymbol{M}$, $\underline{\mathrm{I}}$ with $\underline{\boldsymbol{I}}^{S/S^*}$, $\underline{\mathrm{I}}_p$ with $\underline{\boldsymbol{I}}^{R_i/R_i^*}$, $\Omega$ with ${}^N\boldsymbol{\omega}^B$, $\omega_p$ with ${}^B\boldsymbol{\omega}^{R_i}$, $(\dot{\Omega})_v$ with ${}^N\boldsymbol{\alpha}^B$, and $(\dot{\omega}_p)_p$ with ${}^B\boldsymbol{\alpha}^{R_i}$, it becomes evident that forming dot products with the resulting expression and three vectors ${}^N\boldsymbol{\omega}_r^B$ produces the first three scalar relationships given by Eqs. (7).

#### Dynamical Equations for a Complex Gyrostat

A spacecraft known as a simple gyrostat is described in Sec. 3.6 of Ref. 23; the system $S$ in the preceding discussion becomes a simple gyrostat when the number of flywheels $\mathcal{F}$ is equal to 1 and when no CMGs are present ($\mathcal{C} = 0$ and $\rho = \mathcal{F}$). A spacecraft with more than one flywheel, such as the one shown in Fig. 2, will be referred to

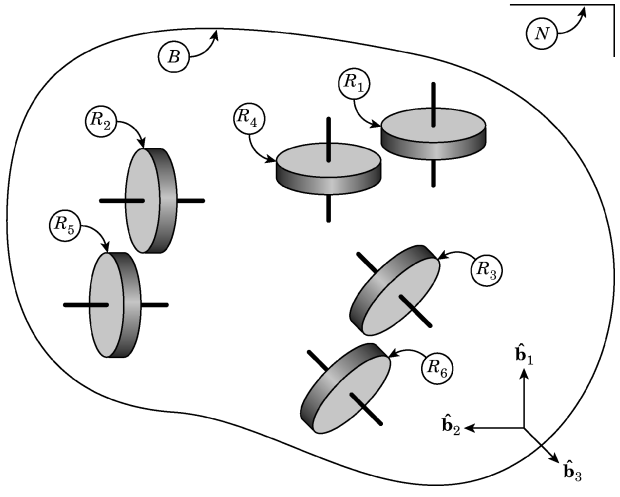


**Fig. 2 Spacecraft with flywheels.**

as a complex gyrostat; equations of motion with $\mathcal{F}=6$ are given in the following material.

Without a great loss of generality, one can at this point work with six flywheel rotors $R_1, \ldots, R_6$ ($\mathcal{F}=6$) arranged in three counter-rotating pairs as shown in Fig. 2, with the spin axes of $R_1$ and $R_4$ parallel to $\hat{\boldsymbol{b}}_1$, $R_2$ and $R_5$ parallel to $\hat{\boldsymbol{b}}_2$, and $R_3$ and $R_6$ parallel to $\hat{\boldsymbol{b}}_3$. The generalized speeds $u_4, \ldots, u_9$ associated with the flywheels are then used to form the angular velocities ${}^B\boldsymbol{\omega}^{R_i}$ of $R_i$ in $B$, $i=1, \ldots, 6$,

$$
\begin{aligned}
&{}^B\boldsymbol{\omega}^{R_1} = u_4\hat{\boldsymbol{b}}_1, \qquad {}^B\boldsymbol{\omega}^{R_2} = u_6\hat{\boldsymbol{b}}_2, \qquad {}^B\boldsymbol{\omega}^{R_3} = u_8\hat{\boldsymbol{b}}_3\\
&{}^B\boldsymbol{\omega}^{R_4} = u_5\hat{\boldsymbol{b}}_1, \qquad {}^B\boldsymbol{\omega}^{R_5} = u_7\hat{\boldsymbol{b}}_2, \qquad {}^B\boldsymbol{\omega}^{R_6} = u_9\hat{\boldsymbol{b}}_3
\end{aligned} \tag{8}
$$

The inertia dyadics for the six flywheel rotors are given by

$$
\underline{\boldsymbol{I}}^{R_i/R_i^*} = \underline{\boldsymbol{I}}^{R_{i+3}/R_{i+3}^*} = J\hat{\boldsymbol{b}}_i\hat{\boldsymbol{b}}_i + K(\underline{\boldsymbol{U}} - \hat{\boldsymbol{b}}_i\hat{\boldsymbol{b}}_i), \qquad i=1,2,3 \tag{9}
$$

where $J$ and $K$ are the central principal moments of inertia of a flywheel rotor for the axis of symmetry and any line perpendicular to the axis of symmetry, respectively. The unit dyadic is denoted by $\underline{\boldsymbol{U}}$ and can be represented, for example, as $\underline{\boldsymbol{U}} = \hat{\boldsymbol{b}}_1\hat{\boldsymbol{b}}_1 + \hat{\boldsymbol{b}}_2\hat{\boldsymbol{b}}_2 + \hat{\boldsymbol{b}}_3\hat{\boldsymbol{b}}_3$.

Henceforth, we regard the moment about $R_i^*$ of forces exerted by $B$ on $R_i$, $\boldsymbol{M}_T^{B/R_i}$, as the sum of two contributions. The first is from a motor–generator and is denoted by $\boldsymbol{M}^{B/R_i}$. The second is due to damping, related by a constant of proportionality $C_d$ to the angular velocity of $R_i$ relative to $B$. Thus, $\boldsymbol{M}_T^{B/R_i} = \boldsymbol{M}^{B/R_i} - C_d\,{}^B\boldsymbol{\omega}^{R_i}$, $i=1, \ldots, 6$.

Unit vectors $\hat{\boldsymbol{b}}_1$, $\hat{\boldsymbol{b}}_2$, and $\hat{\boldsymbol{b}}_3$ are taken to be parallel to central principal axes of inertia of $S$, so that

$$
\underline{\boldsymbol{I}}^{S/S^*} = I_1\hat{\boldsymbol{b}}_1\hat{\boldsymbol{b}}_1 + I_2\hat{\boldsymbol{b}}_2\hat{\boldsymbol{b}}_2 + I_3\hat{\boldsymbol{b}}_3\hat{\boldsymbol{b}}_3 \tag{10}
$$

where $I_1$, $I_2$, and $I_3$ are central principal moments of inertia of $S$. Equations (7) then yield 12 scalar relationships. When the first three are decoupled from the fourth through ninth, they can be written as

$$
\begin{aligned}
(I_1 - 2J)\dot{u}_1 &= (I_2 - I_3)u_2u_3 - J[u_2(u_8+u_9) - u_3(u_6+u_7)] + M_1\\
&\quad - \left(\boldsymbol{M}_1 + \boldsymbol{M}^{B/R_1} + \boldsymbol{M}_4 + \boldsymbol{M}^{B/R_4}\right)\cdot\hat{\boldsymbol{b}}_1 + C_d(u_4+u_5)
\end{aligned} \tag{11}
$$

$$
\begin{aligned}
(I_2 - 2J)\dot{u}_2 &= (I_3 - I_1)u_1u_3 - J[u_3(u_4+u_5) - u_1(u_8+u_9)] + M_2\\
&\quad - \left(\boldsymbol{M}_2 + \boldsymbol{M}^{B/R_2} + \boldsymbol{M}_5 + \boldsymbol{M}^{B/R_5}\right)\cdot\hat{\boldsymbol{b}}_2 + C_d(u_6+u_7)
\end{aligned} \tag{12}
$$

$$
\begin{aligned}
(I_3 - 2J)\dot{u}_3 &= (I_1 - I_2)u_1u_2 - J[u_1(u_6+u_7) - u_2(u_4+u_5)] + M_3\\
&\quad - \left(\boldsymbol{M}_3 + \boldsymbol{M}^{B/R_3} + \boldsymbol{M}_6 + \boldsymbol{M}^{B/R_6}\right)\cdot\hat{\boldsymbol{b}}_3 + C_d(u_8+u_9)
\end{aligned} \tag{13}
$$

$$
J(\dot{u}_1 + \dot{u}_4) = \left(\boldsymbol{M}_1 + \boldsymbol{M}^{B/R_1}\right)\cdot\hat{\boldsymbol{b}}_1 - C_du_4 \tag{14}
$$

$$
J(\dot{u}_1 + \dot{u}_5) = \left(\boldsymbol{M}_4 + \boldsymbol{M}^{B/R_4}\right)\cdot\hat{\boldsymbol{b}}_1 - C_du_5 \tag{15}
$$

$$
J(\dot{u}_2 + \dot{u}_6) = \left(\boldsymbol{M}_2 + \boldsymbol{M}^{B/R_2}\right)\cdot\hat{\boldsymbol{b}}_2 - C_du_6 \tag{16}
$$

$$
J(\dot{u}_2 + \dot{u}_7) = \left(\boldsymbol{M}_5 + \boldsymbol{M}^{B/R_5}\right)\cdot\hat{\boldsymbol{b}}_2 - C_du_7 \tag{17}
$$

$$
J(\dot{u}_3 + \dot{u}_8) = \left(\boldsymbol{M}_3 + \boldsymbol{M}^{B/R_3}\right)\cdot\hat{\boldsymbol{b}}_3 - C_du_8 \tag{18}
$$

$$
J(\dot{u}_3 + \dot{u}_9) = \left(\boldsymbol{M}_6 + \boldsymbol{M}^{B/R_6}\right)\cdot\hat{\boldsymbol{b}}_3 - C_du_9 \tag{19}
$$

$$
m_S\dot{u}_r = F_{r-9} \qquad r = 10, 11, 12 \tag{20}
$$

where the scalars $M_j$ in Eqs. (11–13) are defined by the relationships $M_j \triangleq \boldsymbol{M}\cdot\hat{\boldsymbol{b}}_j$ and $F_j$ in Eqs. (20) are defined as $F_j \triangleq \boldsymbol{F}\cdot\hat{\boldsymbol{n}}_j$, $j=1,2,3$.

Equations (11–20) are, thus, a complete set of nonlinear dynamical equations of motion for a complex gyrostat composed of a body $B$ and six axisymmetric rotors $R_1, \ldots, R_6$ whose mass centers and spin axes are fixed in $B$; the rotors are arranged in pairs, with the spin axes in each pair parallel to each other and to a central principal axis of inertia of the gyrostat.

If a rotor $R_i$ does not possess a magnetic dipole moment and is housed inside $B$ where it is protected from the action of aerodynamic forces, then the principal contribution to the external torque $\boldsymbol{M}_i$ is gravitational moment exerted by the celestial body about which the gyrostat orbits. An expression for an often used approximation of gravitational moment is given in Eq. (2.6.8) of Ref. 23, where it becomes clear that the dot products $\boldsymbol{M}_i\cdot\hat{\boldsymbol{b}}_i$ and $\boldsymbol{M}_{i+3}\cdot\hat{\boldsymbol{b}}_i$, $i=1,2,3$, all vanish because in each case the unit vector $\hat{\boldsymbol{b}}_i$ is parallel to an axis of symmetry of the rotor. After removing rotors $R_1$, $R_2$, $R_4$, $R_5$, and $R_6$ from the picture, and setting $C_d=0$, some manipulation shows that Eqs. (11–13) and (18) reduce to Eqs. (3.7.28–3.7.31) in Ref. 23 for a simple gyrostat in which the spin axis of the single rotor is parallel to $\hat{\boldsymbol{b}}_3$.

**Approximate, Linear Equations for a Spacecraft with Flywheels and CMGs**

In Ref. 5, Wie et al. develop a scheme for controlling a spacecraft's attitude and managing the angular momentum of a collection of CMGs and the results are applied to a space station. They derive equations that describe the motion of a spacecraft with an approximate representation of the effects of the CMGs and then linearize the equations to design a control law. We now extend their approach to include flywheels.

First, we define the resultants of the central angular momenta in $B$ of all flywheels and CMGs as the vectors $\boldsymbol{H}$ and $\boldsymbol{h}$, respectively,

$$
\boldsymbol{H} \triangleq \sum_{i=1}^{\mathcal{F}} {}^B\boldsymbol{H}^{R_i/R_i^*}, \qquad \boldsymbol{h} \triangleq \sum_{i=\mathcal{F}+1}^{\rho} {}^B\boldsymbol{H}^{R_i/R_i^*} \tag{21}
$$

The time derivatives of $\boldsymbol{H}$ and $\boldsymbol{h}$ in $B$ are represented by

$$
\dot{\boldsymbol{H}} \triangleq \frac{{}^B\mathrm{d}}{\mathrm{d}t}\boldsymbol{H}, \qquad \dot{\boldsymbol{h}} \triangleq \frac{{}^B\mathrm{d}}{\mathrm{d}t}\boldsymbol{h} \tag{22}
$$

We then define two vectors $\bar{\boldsymbol{\tau}}$ and $\boldsymbol{\tau}$ that, together, form the first sum in Eqs. (7),

$$
\bar{\boldsymbol{\tau}} \triangleq \dot{\boldsymbol{H}} + {}^N\boldsymbol{\omega}^B \times \boldsymbol{H}, \qquad \boldsymbol{\tau} \triangleq \dot{\boldsymbol{h}} + {}^N\boldsymbol{\omega}^B \times \boldsymbol{h} \tag{23}
$$

The second sum appearing in Eqs. (7) receives contributions only from CMGs and accounts for the time rate of change of CMG mass distribution; it is neglected in comparison to the first sum, based on the assumption that the CMG gimbal speeds are much lower than the rotor spin speed. In addition, central moments and products of inertia of $S$ are regarded as constant in Ref. 5, based on the assumption that reorientation of CMG rotors (and gimbals) does not significantly redistribute system mass. Both assumptions are quite reasonable in the case of the ISS and its four CMGs with constant rotor speeds of 6600 rpm.

We regard the moment $\boldsymbol{M}$ as the sum of two terms, the gravitational moment exerted on $S$ and all other contributions to $\boldsymbol{M}$. When an approximate expression for gravitational moment such as that given by Eq. (2.6.3) in Ref. 23 is used, the first of these can be written as $3\Omega^2\hat{\boldsymbol{r}}\times\underline{\boldsymbol{I}}^{S/S^*}\cdot\hat{\boldsymbol{r}}$, where $\Omega$ is the angular speed of a circular orbit and $\hat{\boldsymbol{r}}$ is a unit position vector from Earth's mass center to $S^*$. All other contributions to $\boldsymbol{M}$ are represented with the vector $\boldsymbol{w}$.

The foregoing discussion allows us to write the first three of Eqs. (7) as

$$
\begin{aligned}
&\left(\underline{\boldsymbol{I}}^{S/S^*}\cdot{}^N\boldsymbol{\alpha}^B\right)\cdot\hat{\boldsymbol{b}}_r\\
&\quad = \left(-{}^N\boldsymbol{\omega}^B\times\underline{\boldsymbol{I}}^{S/S^*}\cdot{}^N\boldsymbol{\omega}^B + 3\Omega^2\hat{\boldsymbol{r}}\times\underline{\boldsymbol{I}}^{S/S^*}\cdot\hat{\boldsymbol{r}} - \boldsymbol{\tau} - \bar{\boldsymbol{\tau}} + \boldsymbol{w}\right)\cdot\hat{\boldsymbol{b}}_r\\
&\qquad\qquad r=1,2,3
\end{aligned} \tag{24}
$$

In the absence of flywheels ($\mathcal{F}=0$ and $\rho=\mathcal{C}$), $\bar{\boldsymbol{\tau}}=\boldsymbol{0}$ and Eqs. (24) reduce to the vector-dyadic representation of the three scalar Eqs. (1) appearing in Ref. 5. Three additional relationships are employed in Ref. 5 as a basis for control law design, namely, their Eqs. (3) that are the scalar equivalents of the second of Eqs. (23) here.

A note is now in order regarding the number of differential equations (7) on the one hand and, on the other hand, the number of differential equations employed in the approach of Ref. 5. The number of dynamical equations of motion (7) is equal to the number $n$ of degrees of freedom of $S$ in $N$, exactly the number required to specify the motion of $S$ completely. Three of these equations describe the translation of $S^*$ and the remaining $n-3$ govern rotational motions of $B$ and the CMG rotors. In contrast, rotational motion is represented in Ref. 5 by just six differential equations, three of Eqs. (1) and three of Eqs. (3), no matter what is the actual value of $n$. However, for the purpose of designing a control law, we adopt this approach and work with Eqs. (23) and (24), representing nine approximate scalar dynamical equations for a spacecraft with flywheels and CMGs.

In addition to these nine differential equations, kinematical differential equations for variables describing the orientation of $B$ in some reference frame are required; it is convenient to choose a local-horizontal–local-vertical reference frame $L$, in which $\hat{\boldsymbol{r}}$ is fixed, where the angular velocity ${}^N\boldsymbol{\omega}^L$ in $N$ has a constant magnitude of $\Omega$. We employ angles belonging to a body-three, 2–3–1 rotation sequence as set forth on p. 423 of Ref. 23. The sequence is also known as pitch–yaw–roll, with the angles denoted by $\theta_1$, $\theta_2$, and $\theta_3$, respectively. The three associated kinematical equations of motion can be written as

$$\dot{\theta}_1 = (C_3u_2 - S_3u_3)/C_2 + \Omega, \qquad \dot{\theta}_2 = S_3u_2 + C_3u_3$$
$$\dot{\theta}_3 = u_1 + S_2(-C_3u_2 + S_3u_3)/C_2 \tag{25}$$

where $S_2 \triangleq \sin\theta_2$, $C_2 \triangleq \cos\theta_2$, and so forth.

It is well known that a single rigid body may move in orbit such that its orientation is fixed in $L$, with the central principal axes of inertia parallel to local vertical $\hat{\boldsymbol{r}}$, local horizontal, and the direction normal to the orbit plane. In the absence of $\boldsymbol{w}$, this orientation is the TEA. As explained in Sec. 3.5 of Ref. 23, such motion is possible when the rigid body travels in a circular orbit and is subject only to the gravitational force and moment exerted by a planet whose mass is uniformly distributed throughout a sphere. The body $B$ of our spacecraft can move in this fashion when $\boldsymbol{w} = \boldsymbol{\tau} = \bar{\boldsymbol{\tau}} = \boldsymbol{0}$, which means, for the last two vectors, that $\boldsymbol{h} = \boldsymbol{H} = \boldsymbol{0}$, the rotor spin speeds do not change, and CMG gimbals do not move. One may linearize "about" this condition with $\hat{\boldsymbol{b}}_i$ parallel to central principal axes of inertia of $S$, where $\hat{\boldsymbol{b}}_3 = -\hat{\boldsymbol{r}}$ when the orientation angles $\theta_i$, $i = 1, 2, 3$, have nominal values of zero. The linearization is prefaced by introducing "perturbations," or quantities assumed to remain small, denoted with a tilde:

$$\theta_i = 0 + \tilde{\theta}_i, \qquad H_i = 0 + \tilde{H}_i, \qquad h_i = 0 + \tilde{h}_i, \qquad i = 1, 2, 3 \tag{26}$$

where $H_i \triangleq \boldsymbol{H} \cdot \hat{\boldsymbol{b}}_i$ and $h_i \triangleq \boldsymbol{h} \cdot \hat{\boldsymbol{b}}_i$, $i = 1, 2, 3$. In addition, $\tilde{u}_1$, $\tilde{u}_2$, and $\tilde{u}_3$ are introduced as perturbations of the angular speeds of $B$ in $N$,

$$u_1 = 0 + \tilde{u}_1, \qquad u_2 = -\Omega + \tilde{u}_2, \qquad u_3 = 0 + \tilde{u}_3 \tag{27}$$

Equations (23–25), linearized in the perturbations, are written as

$$I_1\dot{\tilde{u}}_1 = (I_3 - I_2)\left(3\Omega^2\tilde{\theta}_3 + \Omega\tilde{u}_3\right) - \tau_1 - \bar{\tau}_1 + w_1 \tag{28}$$

$$I_2\dot{\tilde{u}}_2 = (I_3 - I_1)\left(3\Omega^2\tilde{\theta}_1\right) - \tau_2 - \bar{\tau}_2 + w_2 \tag{29}$$

$$I_3\dot{\tilde{u}}_3 = (I_2 - I_1)\Omega\tilde{u}_1 - \tau_3 - \bar{\tau}_3 + w_3 \tag{30}$$

$$\dot{\tilde{h}}_1 = \Omega\tilde{h}_3 + \tau_1, \qquad \dot{\tilde{h}}_2 = \tau_2, \qquad \dot{\tilde{h}}_3 = -\Omega\tilde{h}_1 + \tau_3 \tag{31}$$

$$\dot{\tilde{H}}_1 = \Omega\tilde{H}_3 + \bar{\tau}_1, \qquad \dot{\tilde{H}}_2 = \bar{\tau}_2, \qquad \dot{\tilde{H}}_3 = -\Omega\tilde{H}_1 + \bar{\tau}_3 \tag{32}$$

$$\dot{\tilde{\theta}}_1 = \tilde{u}_2, \qquad \dot{\tilde{\theta}}_2 = \tilde{u}_3 - \Omega\tilde{\theta}_3, \qquad \dot{\tilde{\theta}}_3 = \tilde{u}_1 + \Omega\tilde{\theta}_2 \tag{33}$$

where $\tau_i \triangleq \boldsymbol{\tau} \cdot \hat{\boldsymbol{b}}_i$, $\bar{\tau}_i \triangleq \bar{\boldsymbol{\tau}} \cdot \hat{\boldsymbol{b}}_i$, and $w_i \triangleq \boldsymbol{w} \cdot \hat{\boldsymbol{b}}_i$, $i = 1, 2, 3$.

## Attitude Control

The TEA of a spacecraft is defined as the orientation for which the angular acceleration of $B$ in $N$ vanishes. The present ISS attitude and CMG momentum control algorithm can keep the orientation in the neighborhood of a time-varying TEA almost indefinitely, without requiring any expenditure of propellant from the reaction control system. A law for controlling the orientation of $B$ in $L$, together with the momentum of flywheels and CMGs, has been designed using the infinite-horizon linear quadratic regulator (LQR) technique in which a scalar quadratic performance index given by

$$\mathcal{P} = \int_0^\infty (\{x\}^T[Q]\{x\} + \{\tau\}^T[R]\{\tau\})\,\mathrm{d}t \tag{34}$$

is minimized subject to the linear differential equations

$$\{\dot{x}\} = [A]\{x\} + [B]\{\tau\} \tag{35}$$

The technique yields a state feedback gain matrix $[K]$ used in turn to obtain $\{\tau\}$,

$$\{\tau\} = -[K]\{x\} \tag{36}$$

As mentioned in the Introduction, a controller will seek a TEA when spacecraft attitude and angular speed, as well as flywheel and CMG momentum, are included in the cost function $\mathcal{P}$. Although such a controller will minimize the magnitudes of $\boldsymbol{h}$ and $\boldsymbol{H}$, integrals of momentum

$$\int \tilde{h}_i\,\mathrm{d}t, \qquad \int \tilde{H}_i\,\mathrm{d}t \qquad i = 1, 2, 3$$

must also be included in $\mathcal{P}$ to eliminate momentum bias, as is done in Ref. 5. Thus, seeking a TEA is accomplished by regulating the states contained in the $18 \times 1$ column matrix,

$$\{x\} = \left[\theta_1^*, \theta_2^*, \theta_3^*, u_1^*, \ldots, h_1^*, \ldots, H_1^*, \ldots, \int h_1^*\,\mathrm{d}t^*, \ldots, \int H_1^*\,\mathrm{d}t^*, \ldots\right]^T \tag{37}$$

where the superscript $T$ indicates the transpose of a matrix and the superscript asterisk indicates the states are made nondimensional according to the following definitions to eliminate numerical difficulties in obtaining $[K]$:

$$\theta_i^* \triangleq \tilde{\theta}_i, \qquad u_i^* \triangleq \tilde{u}_i/\Omega, \qquad h_i^* \triangleq \tilde{h}_i/I_i\,\Omega, \qquad H_i^* \triangleq \tilde{H}_i/I_i\,\Omega$$
$$i = 1, 2, 3 \tag{38}$$

$$t^* \triangleq \Omega t \tag{39}$$

When Eqs. (35) are nondimensionalized in this way, the derivative of $\{x\}$ is taken with respect to nondimensional time $t^*$. The column matrix $\{\tau\}$ is dimensioned $6 \times 1$ with the elements

$$\{\tau\} \triangleq \left[\tau_1^* \quad \tau_2^* \quad \tau_3^* \quad \bar{\tau}_1^* \quad \bar{\tau}_2^* \quad \bar{\tau}_3^*\right]^T \tag{40}$$

defined as

$$\tau_i^* \triangleq \tau_i \big/ I_i\,\Omega^2, \qquad \bar{\tau}_i^* \triangleq \bar{\tau}_i \big/ I_i\,\Omega^2, \qquad i = 1, 2, 3 \tag{41}$$

Thus, the nondimensional forms of Eqs. (28–33), supplemented with appropriate differential equations for

$$\int h_i^*\,\mathrm{d}t^*, \qquad \int H_i^*\,\mathrm{d}t^*$$

play the part of Eqs. (35). The variables $w_1$, $w_2$, and $w_3$ are set to zero in Eqs. (28–30) for the control law design, which means that

**Table 1 Values used to construct [$Q$]**

| Parameter, $i = 1, 2, 3$ | Value |
|---|---|
| $\tilde{\theta}_i$ | 1 deg |
| $\tilde{u}_i$ | 0.2 deg/s |
| $\tilde{h}_i$ | 6,779 N · m · s |
| $\tilde{H}_i$ | 6,779 N · m · s |
| $\int \tilde{h}_i \, dt$ | $2.7 \times 10^6$ N · m · s$^2$ |
| $\int \tilde{H}_i \, dt$ | $2.7 \times 10^6$ N · m · s$^2$ |

$\boldsymbol{w}$ will be an unmodeled disturbance torque as far as the controller is concerned.

As suggested by Bryson and Ho in Ref. 24, the weighting matrix $[Q]$ can be chosen as diagonal, and unity should be approximately equal to the product of $Q_{jj}$ and the square of the maximum acceptable value of the associated element $x_j$ of $\{x\}$. The values listed in Table 1 have been found to result in reasonable closed-loop pole locations and typical TEA-seeking attitude motion. Before constructing $[Q]$, the values in Table 1 must be made nondimensional to be in correspondence with the elements of $\{x\}$. Likewise, a diagonal form of $[R]$ is convenient, with unity approximately equal to the product of $R_{kk}$ and the square of the maximum acceptable value of the associated element of $\{\tau\}$, $k = 1, \ldots, 6$. The value of each element of $\{\tau\}$ is taken to be 2.7 N · m, which must be nondimensionalized before constructing $[R]$.

The matrices $[A]$, $[Q]$, $[B]$, and $[R]$ are dimensioned $18 \times 18$, $18 \times 18$, $18 \times 6$, and $6 \times 6$, respectively, in accordance with the number of control variables and regulated state variables for this control scheme.

## Flywheel Steering Laws

The great benefit of utilizing flywheels is that they can serve simultaneously as attitude control actuators and as energy storage devices. This dual role requires that $\bar{\boldsymbol{\tau}}$, obtained on the basis of attitude control considerations, be applied in a way that allows energy to be stored or discharged as needed. A flywheel rotor $R_i$ is suspended in a vacuum housing in $B$ with magnetic bearings, and relative motion between $R_i$ and $B$ is brought about by a motor–generator that enables $B$ to exert on $R_i$ a torque with magnitude $\boldsymbol{M}^{B/R_i} \cdot \hat{\boldsymbol{\beta}}_i$, the purpose of which is to produce and change rotor momentum to furnish attitude control and to alter the rotor's rotational kinetic energy. The capacity for energy storage is often characterized in terms of the power delivered during discharge, or the rate at which rotational kinetic energy is changed. In this section, relationships for $\boldsymbol{M}^{B/R_i} \cdot \hat{\boldsymbol{\beta}}_i$ as functions of power, $\bar{\boldsymbol{\tau}}$, and rotor speeds are developed; they are referred to collectively as a flywheel steering law because they are similar in nature to a CMG steering law that determines gimbal speeds (and thus, indirectly, gimbal motor torques) needed to produce $\boldsymbol{\tau}$ as requested by a control law. Two such steering laws are presented: The first is the result of simply prescribing the total power of the flywheel system, whereas specification of the power required for each of three flywheel pairs gives rise to the second law. Bearing friction and damping are neglected in the design of the steering laws.

The flywheel rotors are arranged in counter-rotating pairs; each pair, denoted by $F_i$, consists of rotors $R_i$ and $R_{i+3}$, $i = 1, 2, 3$. With reference to Eq. (5) of Ref. 25, the power ${}^B P^{F_i}$ of $F_i$ in $B$ can be expressed as

$$ {}^B P^{F_i} = \left(\underline{\boldsymbol{I}}^{R_i/R_i^*} \cdot {}^B\boldsymbol{\alpha}^{R_i}\right) \cdot {}^B\boldsymbol{\omega}^{R_i} + \left(\underline{\boldsymbol{I}}^{R_{i+3}/R_{i+3}^*} \cdot {}^B\boldsymbol{\alpha}^{R_{i+3}}\right) \cdot {}^B\boldsymbol{\omega}^{R_{i+3}} \qquad i = 1, 2, 3 \quad (42) $$

or, in view of Eqs. (8) and (9),

$$ {}^B P^{F_i} = J(\dot{u}_{2i+2} u_{2i+2} + \dot{u}_{2i+3} u_{2i+3}), \qquad i = 1, 2, 3 \quad (43) $$

and, therefore, the total power may be expressed as

$$ {}^B P^F \triangleq \sum_{i=1}^{3} {}^B P^{F_i} = J \sum_{i=1}^{3} (\dot{u}_{2i+2} u_{2i+2} + \dot{u}_{2i+3} u_{2i+3}) \quad (44) $$

Now, if $\dot{u}_1$, $\dot{u}_2$, and $\dot{u}_3$ are assumed to be small in comparison to $\dot{u}_4, \ldots, \dot{u}_9$, $C_d$ is neglected, and $\boldsymbol{M}_i \cdot \hat{\boldsymbol{b}}_i$ and $\boldsymbol{M}_{i+3} \cdot \hat{\boldsymbol{b}}_i$, $i = 1, 2, 3$ vanish for the reasons put forth earlier, then Eqs. (14–19) may be approximated as

$$ J\dot{u}_{2i+2} \approx \boldsymbol{M}^{B/R_i} \cdot \hat{\boldsymbol{b}}_i, \qquad J\dot{u}_{2i+3} \approx \boldsymbol{M}^{B/R_{i+3}} \cdot \hat{\boldsymbol{b}}_i, \qquad i = 1, 2, 3 \quad (45) $$

Together with the first of Eqs. (22) and (23), these lead to

$$ (\bar{\boldsymbol{\tau}} - {}^N\boldsymbol{\omega}^B \times \boldsymbol{H}) \cdot \hat{\boldsymbol{b}}_i = \dot{H}_i = J(\dot{u}_{2i+2} + \dot{u}_{2i+3}) \approx \left(\boldsymbol{M}^{B/R_i} + \boldsymbol{M}^{B/R_{i+3}}\right) \cdot \hat{\boldsymbol{b}}_i, \qquad i = 1, 2, 3 \quad (46) $$

or

$$ \boldsymbol{M}^{B/R_{i+3}} \cdot \hat{\boldsymbol{b}}_i \approx \left(\bar{\boldsymbol{\tau}} - {}^N\boldsymbol{\omega}^B \times \boldsymbol{H} - \boldsymbol{M}^{B/R_i}\right) \cdot \hat{\boldsymbol{b}}_i \qquad i = 1, 2, 3 \quad (47) $$

Substitution from Eqs. (45) into Eq. (44) produces

$$ {}^B\boldsymbol{P}^F \approx \sum_{i=1}^{3} \left(u_{2i+2} \boldsymbol{M}^{B/R_i} + u_{2i+3} \boldsymbol{M}^{B/R_{i+3}}\right) \cdot \hat{\boldsymbol{b}}_i \quad (48) $$

### Pseudoinverse Steering Law

Equations (47) and (48) constitute a system of four equations, linear in the six unknowns $\boldsymbol{M}^{B/R_i} \cdot \hat{\boldsymbol{b}}_i$ and $\boldsymbol{M}^{B/R_{i+3}} \cdot \hat{\boldsymbol{b}}_i$, $i = 1, 2, 3$. This underdetermined system can be written in matrix form as

$$ [A_s]\{y\} = \{z\} \quad (49) $$

where

$$ [A_s] \triangleq \begin{bmatrix} 1 & 1 & 0 & 0 & 0 & 0 \\ 0 & 0 & 1 & 1 & 0 & 0 \\ 0 & 0 & 0 & 0 & 1 & 1 \\ u_4 & u_5 & u_6 & u_7 & u_8 & u_9 \end{bmatrix} \quad (50) $$

$$ \{y\} \triangleq \left[\boldsymbol{M}^{B/R_1} \cdot \hat{\boldsymbol{b}}_1 \quad \boldsymbol{M}^{B/R_4} \cdot \hat{\boldsymbol{b}}_1 \quad \boldsymbol{M}^{B/R_2} \cdot \hat{\boldsymbol{b}}_2 \quad \boldsymbol{M}^{B/R_5} \cdot \hat{\boldsymbol{b}}_2 \quad \boldsymbol{M}^{B/R_3} \cdot \hat{\boldsymbol{b}}_3 \quad \boldsymbol{M}^{B/R_6} \cdot \hat{\boldsymbol{b}}_3\right]^T \quad (51) $$

$$ \{z\} \triangleq \left[(\bar{\boldsymbol{\tau}} - {}^N\boldsymbol{\omega}^B \times \boldsymbol{H}) \cdot \hat{\boldsymbol{b}}_1 \quad (\bar{\boldsymbol{\tau}} - {}^N\boldsymbol{\omega}^B \times \boldsymbol{H}) \cdot \hat{\boldsymbol{b}}_2 \quad (\bar{\boldsymbol{\tau}} - {}^N\boldsymbol{\omega}^B \times \boldsymbol{H}) \cdot \hat{\boldsymbol{b}}_3 \quad {}^B\boldsymbol{P}^F\right]^T \quad (52) $$

One may solve Eqs. (49) by forming a matrix pseudoinverse such as the one presented in Ref. 26 and developed by Moore and Penrose for underdetermined systems,

$$ [A_s]^+ \triangleq [A_s]^T \left([A_s][A_s]^T\right)^{-1} \quad (53) $$

as long as $[A_s]$ is full rank. The solution

$$\{y\} = [A_s]^+ \{z\} \tag{54}$$

minimizes the sum of the squares of the unknowns, $\{y\}^T\{y\}$. (There exist several other performance measures that could be considered in solving an underdetermined system of equations.) Use of a pseudoinverse is in essence the suggestion made by Hall in Sec. 4 of Ref. 10, which yields a steering law wherein the power and attitude control requirements are met simultaneously, and a function of the instantaneous motor torques, the sum

$$\sum_{i=1}^{3} \left[ \left( \boldsymbol{M}^{B/R_i} \cdot \hat{\boldsymbol{b}}_i \right)^2 + \left( \boldsymbol{M}^{B/R_{i+3}} \cdot \hat{\boldsymbol{b}}_i \right)^2 \right]$$

is minimized.

With the definitions

$$d_1 \triangleq u_5 - u_4, \qquad d_2 \triangleq u_7 - u_6, \qquad d_3 \triangleq u_9 - u_8 \tag{55}$$

$$s_1 \triangleq u_5 + u_4, \qquad s_2 \triangleq u_7 + u_6, \qquad s_3 \triangleq u_9 + u_8 \tag{56}$$

the pseudoinverse in Eq. (53) can be written explicitly as

$$[A_s]^+ = \frac{1}{2\left(d_1^2 + d_2^2 + d_3^2\right)} \begin{bmatrix} 2u_5 d_1 + d_2^2 + d_3^2 & s_2 d_1 & s_3 d_1 & -2d_1 \\ -2u_4 d_1 + d_2^2 + d_3^2 & -s_2 d_1 & -s_3 d_1 & 2d_1 \\ s_1 d_2 & 2u_7 d_2 + d_1^2 + d_3^2 & s_3 d_2 & -2d_2 \\ -s_1 d_2 & -2u_6 d_2 + d_1^2 + d_3^2 & -s_3 d_2 & 2d_2 \\ s_1 d_3 & s_2 d_3 & 2u_9 d_3 + d_1^2 + d_2^2 & -2d_3 \\ -s_1 d_3 & -s_2 d_3 & -2u_8 d_3 + d_1^2 + d_2^2 & 2d_3 \end{bmatrix} \tag{57}$$

Note that, if the rotor speed differences $d_1$, $d_2$, and $d_3$ vanish for all three flywheel pairs, the pseudoinverse becomes infinite and the steering law does not furnish a result. Because the rotor speeds of the flywheels in each pair will normally have opposite signs, this condition should be unlikely. In addition, examination of Eqs. (51), (52), (54), and (57) reveals that, when the flywheels are not required to provide attitude control, $\bar{\boldsymbol{\tau}} = \boldsymbol{0}$, and the condition of counter-rotation is present ($u_{2i+3} = -u_{2i+2}$, thus $\boldsymbol{H} = \boldsymbol{0}$), this steering law dictates that $\boldsymbol{M}^{B/R_{i+3}} \cdot \hat{\boldsymbol{b}}_i = -\boldsymbol{M}^{B/R_i} \cdot \hat{\boldsymbol{b}}_i$, and counter-rotation is preserved.

#### Divided-Power Steering Law

As an alternative to dealing with the four Eqs. (47) and (48), one could replace the single Eq. (48) with three others by choosing to divide the power requirement evenly among the three flywheel pairs, ${}^B P^{F_1} = {}^B P^{F_2} = {}^B P^{F_3} = \frac{1}{3} {}^B P^F$, yielding six equations in six unknowns. We refer to the result of this approach as the divided power steering law because the power requirement is divided into three equal parts. Substitution from Eqs. (45) into Eqs. (43) gives the three new equations

$${}^B P^{F_i} \approx \left( u_{2i+2} \boldsymbol{M}^{B/R_i} + u_{2i+3} \boldsymbol{M}^{B/R_{i+3}} \right) \cdot \hat{\boldsymbol{b}}_i, \qquad i = 1, 2, 3 \tag{58}$$

Now, substitution from Eqs. (47) with subsequent rearrangement of the result yields

$$\boldsymbol{M}^{B/R_i} \cdot \hat{\boldsymbol{b}}_i = \frac{{}^B P^{F_i} - u_{2i+3}(\bar{\boldsymbol{\tau}} - {}^N\boldsymbol{\omega}^B \times \boldsymbol{H}) \cdot \hat{\boldsymbol{b}}_i}{u_{2i+2} - u_{2i+3}}, \qquad i = 1, 2, 3 \tag{59}$$

and, when one substitutes from this expression into Eqs. (47), the result is

$$\boldsymbol{M}^{B/R_{i+3}} \cdot \hat{\boldsymbol{b}}_i = \frac{u_{2i+2}(\bar{\boldsymbol{\tau}} - {}^N\boldsymbol{\omega}^B \times \boldsymbol{H}) \cdot \hat{\boldsymbol{b}}_i - {}^B P^{F_i}}{u_{2i+2} - u_{2i+3}}, \qquad i = 1, 2, 3 \tag{60}$$

Equations (59) and (60) constitute another flywheel steering law, indicating the moment that must be applied by a motor–generator to each of two rotors belonging to a counter-rotating pair to apply $\bar{\boldsymbol{\tau}}$ as called for by an attitude control law and at the same time satisfy power requirements specified by ${}^B P^{F_i}$. Each flywheel pair is expected to operate with the sign of the rotor speed $u_{2i+3}$ opposite the sign of $u_{2i+2}$; hence, the denominators $u_{2i+2} - u_{2i+3} = -d_i$ should remain well away from zero. In this respect, the pseudoinverse steering law may enjoy an advantage because singularity does not occur unless $d_1$, $d_2$, and $d_3$ vanish simultaneously, whereas two of Eqs. (59) and (60) become singular if one of these vanish individually. The objective of the TEA-seeking attitude control law is to maintain an equilibrium attitude where, by definition, the necessary control torque and the flywheel momentum in each axis remain small. The consequence of this is that $-d_i$ is kept as far from zero as possible. Of course, when the disturbance torque environment and power profile are inappropriate to the momentum and kinetic energy capacity of the flywheels, saturation is possible. Therefore, the flywheel system should be properly sized for the vehicle on which it is expected to serve. In the event that the flywheels are not required to participate in attitude control, and the condition of counter-rotation is present, the steering law yields $\boldsymbol{M}^{B/R_{i+3}} \cdot \hat{\boldsymbol{b}}_i = -\boldsymbol{M}^{B/R_i} \cdot \hat{\boldsymbol{b}}_i$ and, thus, maintains the condition of counter-rotation.

## Energy Feedback

The power possessed by the flywheels, given in Eq. (44), can differ from the required value when $C_d \neq 0$. If left unchecked, such unwanted resistance or damping will lead to a deterioration in ${}^B P^F$ that increases with time, to rotor speeds that exceed their maximum and minimum limits, and to singularities in the steering laws. These deleterious effects of damping can be eliminated by the control system through feedback of rotational kinetic energy error.

The total rotational kinetic energy ${}^B K^F$ of the flywheel rotors relative to $B$ can be expressed as

$${}^B K^F = \frac{J}{2} \sum_{i=4}^{9} u_i^2 \tag{61}$$

and the power of $F$ in $B$ is given by the derivative of ${}^B K^F$ with respect to $t$,

$${}^B P^F = \frac{\mathrm{d}}{\mathrm{d}t} {}^B K^F \tag{62}$$

One can regard the required power ${}^B \bar{P}^F$ as the time derivative of a required kinetic energy of $F$ in $B$

$${}^B \bar{P}^F = \frac{\mathrm{d}}{\mathrm{d}t} {}^B \bar{K}^F \tag{63}$$

and define a kinetic energy error $e_k$ as the quantity

$$e_k \triangleq {}^{B}K^{F} - {}^{B}\bar{K}^{F} \tag{64}$$

that is governed by the differential equation

$$\dot{e}_k = \frac{\mathrm{d}}{\mathrm{d}t}({}^{B}K^{F} - {}^{B}\bar{K}^{F}) = {}^{B}P^{F} - {}^{B}\bar{P}^{F} \triangleq e_p \tag{65}$$

where $e_p$ is defined to be the error in power, or the difference between the actual and required values. The LQR technique can be used to control the kinetic energy error by minimizing the cost function,

$$\mathcal{P}_E = \int_0^\infty \left(\lambda\, e_k^2 + e_p^2\right) \mathrm{d}t \tag{66}$$

where $\lambda$ is a weighting parameter on the kinetic energy error of the flywheel system. This leads to a feedback controller in which the required power is adjusted by the amount $-(\sqrt{\lambda})e_k$. Thus, the commanded power is defined to be

$${}^{B}P_c^{F} \triangleq {}^{B}\bar{P}^{F} - \sqrt{\lambda}\, e_k \tag{67}$$

and is used in place of ${}^{B}P^{F}$ in Eq. (52) for the pseudoinverse steering law. Similarly, a commanded power ${}^{B}P_c^{F_i}$, $i = 1, 2, 3$, is obtained for each of the three flywheel pairs and used together with Eqs. (59) and (60) for the divided power steering law. The merits of this kinetic energy error feedback are illustrated presently.

The foregoing approach is similar to that described in Ref. 27, in which an error signal formed from the difference between the ideal and actual speed of each wheel is separately amplified and fed back to the appropriate motor–generator to command higher torque that counteracts damping. The kinetic energy error feedback method is superior in that the motor torques are determined by the flywheel steering law, and thus, compensation for damping is obtained in an optimal sense by minimizing the motor torques. Furthermore, the use of a single global feedback loop greatly simplifies the implementation of the control system, especially when a large number of flywheels are carried by a spacecraft such as the ISS.

## Numerical Simulations

Numerical simulations are performed to demonstrate the efficacy of a comprehensive control system formed by the combination of the LQR for attitude control and momentum management, a flywheel steering law, and kinetic energy error feedback. First, TEA-seeking behavior without feedback of kinetic energy error is examined to illustrate the consequences of failing to counteract damping. Second, the advantages of kinetic energy error feedback are demonstrated. Finally, the performances of the pseudoinverse and the divided power steering laws are compared in some detail.

Simulation results are obtained from numerical solution of the nonlinear differential equations (11–13) with $\tau_r$, $r = 1, 2, 3$, subtracted from the right-hand sides to include the effects of the CMGs, Eqs. (14–19), three scalar differential equations obtained from the second of Eqs. (23), and four kinematical differential equations for quaternion elements in place of Eqs. (25). The dot products $\boldsymbol{M}_i \cdot \hat{\boldsymbol{b}}_i$ and $\boldsymbol{M}_{i+3} \cdot \hat{\boldsymbol{b}}_i$, $i = 1, 2, 3$, in Eqs. (11–19) are neglected for the reasons discussed earlier. The external moment $\boldsymbol{M}$ acting on $S$ is regarded as the sum of the gravitational moment and $\boldsymbol{w}$, the moment about $S^*$ of aerodynamic forces exerted on $S$ when the attitude is near TEA. We use the value of $\boldsymbol{w}$ reported in Ref. 5 for the phase 1 configuration of ISS, given by

$$\boldsymbol{w} = 1.36\Big[\big(1 + \sin\Omega t + \tfrac{1}{2}\sin 2\Omega t\big)\hat{\boldsymbol{b}}_1 + \big(4 + 2\sin\Omega t + \tfrac{1}{2}\sin 2\Omega t\big)\hat{\boldsymbol{b}}_2 + \big(1 + \sin\Omega t + \tfrac{1}{2}\sin 2\Omega t\big)\hat{\boldsymbol{b}}_3\Big]\ \mathrm{N}\cdot\mathrm{m} \tag{68}$$

where $\Omega$, the magnitude of ${}^{N}\boldsymbol{\omega}^{L}$, is taken to be 0.001131 rad/s.

Moments and products of inertia of $S$ with respect to $S^*$ are taken to be

$$[I^{S/S^*}] = 1.36 \times \begin{bmatrix} 50.28 & -0.39 & -0.24 \\ -0.39 & 10.80 & 0.16 \\ -0.24 & 0.16 & 58.57 \end{bmatrix} \times 10^6\ \mathrm{kg}\cdot\mathrm{m}^2 \tag{69}$$

the same values (in metric units) as those associated with phase 1 in Table 1 of Ref. 5, with the exception of $I_{13}$, which is suspected to be a typographical error, the correct value being $-0.24 \times 10^6$ slug $\cdot$ ft$^2$. (The English unit of slug square foot is the unit that is in Ref. 5.)

Each flywheel pair in the FESS is required to discharge 4400 W of power during the portion of the orbit that lies within the Earth's shadow, known as the period of eclipse. The remaining portion of the orbit, during which sunlight reaches the spacecraft, is taken to be twice as long as the eclipse. Therefore, for each orbit, the total power that must be supplied by the 48 pairs of flywheels in the physical system is given by

$${}^{B}\bar{P}^{F} = \begin{cases} 48 \times 2200\ \mathrm{W} = 105.6\ \mathrm{kW}, & 0 \le t \le \frac{2}{3}(2\pi/\Omega) \\ 48 \times -4400\ \mathrm{W} = -211.2\ \mathrm{kW}, & \frac{2}{3}(2\pi/\Omega) \le t \le 2\pi/\Omega \end{cases} \tag{70}$$

for charge and discharge, respectively, where the bar over $P$ indicates a known function of $t$ to be used in connection with the pseudoinverse steering law developed earlier. With the divided power law ${}^{B}\bar{P}^{F_1} = {}^{B}\bar{P}^{F_2} = {}^{B}\bar{P}^{F_3} = \frac{1}{3}{}^{B}\bar{P}^{F}$, therefore,

$${}^{B}\bar{P}^{F_i} = \begin{cases} 35.2\ \mathrm{kW}, & 0 \le t \le \frac{2}{3}(2\pi/\Omega) \\ -70.4\ \mathrm{kW}, & \frac{2}{3}(2\pi/\Omega) \le t \le 2\pi/\Omega \end{cases} \qquad i = 1, 2, 3 \tag{71}$$

for charge and discharge, respectively.

The FESS would have been made up of 96 flywheels. Because the present model involves only 6 rotors, a scaling factor of $96/6 = 16$ is used; thus, $J = 16 \times 0.3010\ \mathrm{kg}\cdot\mathrm{m}^2 = 4.82\ \mathrm{kg}\cdot\mathrm{m}^2$.

The simulation results discussed in the remainder of this section are obtained with the following initial values of the state variables. Angles describing the orientation of $B$ in $L$ at $t = t_0$ are $\theta_1(t_0) = 5$ deg (pitch), $\theta_2(t_0) = 5$ deg (yaw), and $\theta_3(t_0) = 5$ deg (roll). Angular speeds associated with ${}^{N}\boldsymbol{\omega}^{B}$ (with ${}^{L}\boldsymbol{\omega}^{B} = \boldsymbol{0}$) are $u_1(t_0) = -9.86 \times 10^{-5}$ rad/s, $u_2(t_0) = -1.12 \times 10^{-3}$ rad/s, and $u_3(t_0) = 9.82 \times 10^{-5}$ rad/s. Rotor spin speeds are $u_4(t_0) = u_6(t_0) = u_8(t_0) = -20,000$ rpm and $u_5(t_0) = u_7(t_0) = u_9(t_0) = 20,000$ rpm. Initial values of CMG momentum measure numbers are $h_1(t_0) = h_2(t_0) = h_3(t_0) = 0$.

### Damped Flywheel Rotors

The detrimental effects of damping are brought to light by performing a simulation with an illustrative value of $C_d = 10^{-5}\ \mathrm{N}\cdot\mathrm{m}\cdot\mathrm{s}$. One might be tempted to neglect such a seemingly small effect, especially over the short term, but it is shown here to be troublesome if not dealt with over long periods. The performance of the TEA-seeking control law without feedback of kinetic energy error is shown in Figs. 3–7.

Figure 3 shows the time history of the attitude angles and the inertial angular velocity. The solid curve is used for $\theta_1$ (pitch), the dashed curve for $\theta_2$ (yaw), and the dash–dot curve is used for $\theta_3$ (roll). The average values of these orientation angles in the steady state are referred to as average torque equilibrium attitude angles, and they are approximately the same as those shown in Ref. 5, −7.5 deg in pitch, −1.2 deg in yaw, and −0.2 deg in roll. The amplitudes of the steady-state oscillations can be reduced significantly with cyclic disturbance rejection filters, as shown in Ref. 5. Figure 3b shows the inertial angular velocity response, with $u_1$, $u_2$, and $u_3$, shown with solid, dashed, and dash–dot curves, respectively.

Figure 4a shows the progression of the magnitudes of CMG momentum $\boldsymbol{h}$ and Fig. 4b shows flywheel momentum $\boldsymbol{H}$. The former

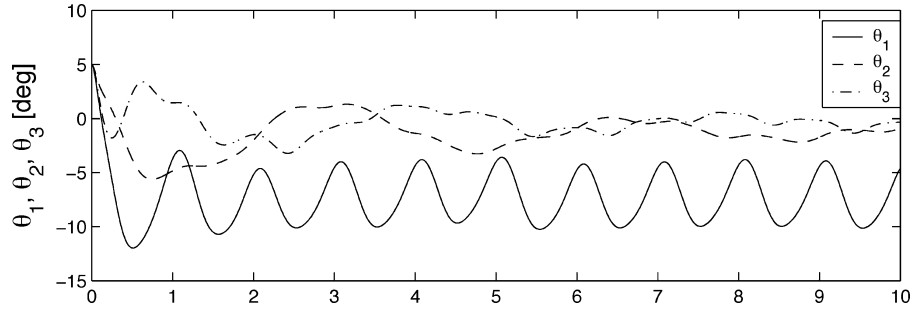


**a) Attitude of $B$ in $L$**

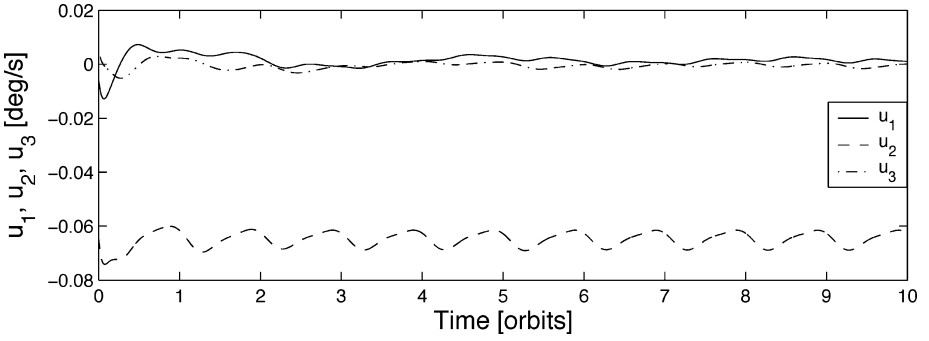


**b) Angular velocity of $B$ in $N$, ${}^{N}\boldsymbol{\omega}^{B}$**

**Fig. 3 Attitude and angular velocity with damped flywheel rotors, without kinetic energy error feedback.**

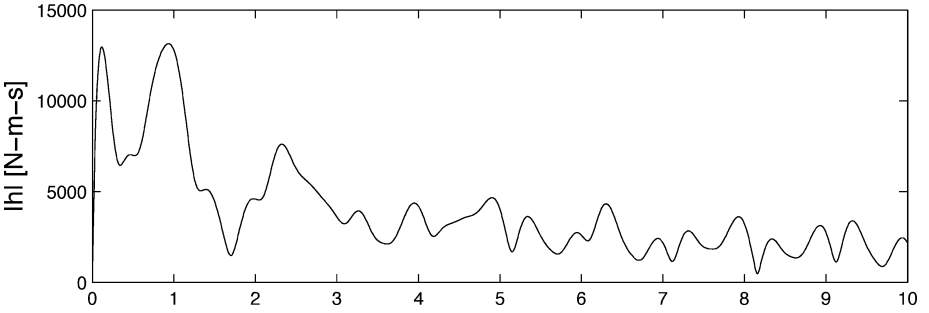


**a) CMG momentum magnitude**

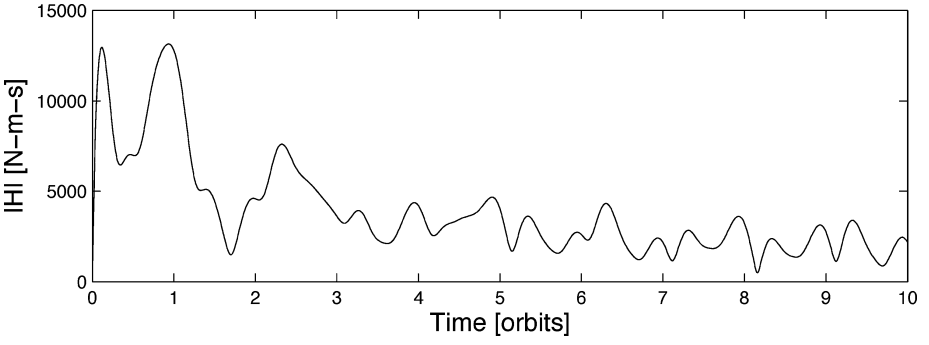


**b) Flywheel momentum magnitude**

**Fig. 4 Momentum magnitude with damped flywheel rotors, without kinetic energy error feedback.**

is obtained from numerical integration of the differential equations represented by the second of Eqs. (23), whereas the latter is simply the magnitude of $J[(u_4+u_5)\hat{\boldsymbol{b}}_1+(u_6+u_7)\hat{\boldsymbol{b}}_2+(u_8+u_9)\hat{\boldsymbol{b}}_3]$. The CMG momentum magnitude remains well below 14,000 $\mathrm{N}\cdot\mathrm{m}\cdot\mathrm{s}$ over the first orbit and in the steady state remains well below 4745 $\mathrm{N}\cdot\mathrm{m}\cdot\mathrm{s}$, the capacity of a single ISS CMG. The similarity of the two curves in Fig. 4 is to be expected because the gains were obtained by weighting

$$\tilde{h}_i, \qquad \int \tilde{h}_i \, \mathrm{d}t, \qquad \tau_i$$

the same as

$$\tilde{H}_i, \qquad \int \tilde{H}_i \, \mathrm{d}t, \qquad \bar{\tau}_i$$

respectively, $i = 1, 2, 3$.

Figure 5a contains the actual power delivered to the spacecraft by the flywheel system as a function of time. Figure 5b shows the error between the actual power and the required power due to the damping in the flywheel system, leading to the large secular kinetic energy loss of more than 50,000 kJ after 10 orbits, shown in Fig. 5c.

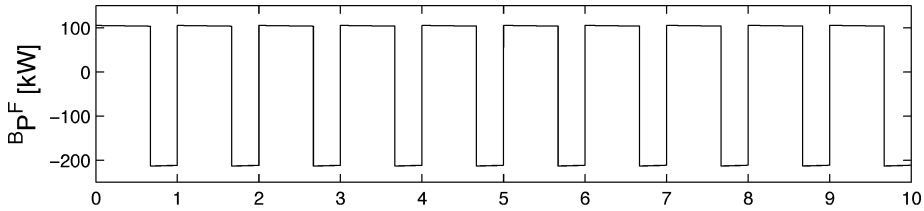


**a) Total actual power**

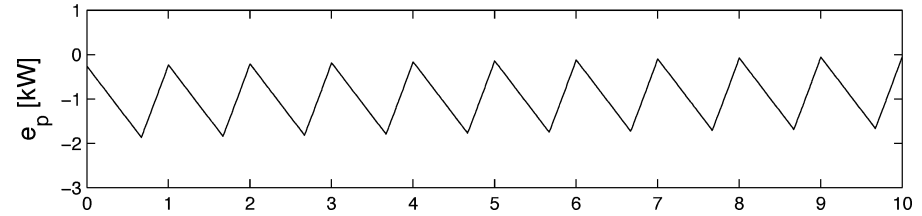


**b) Power error**

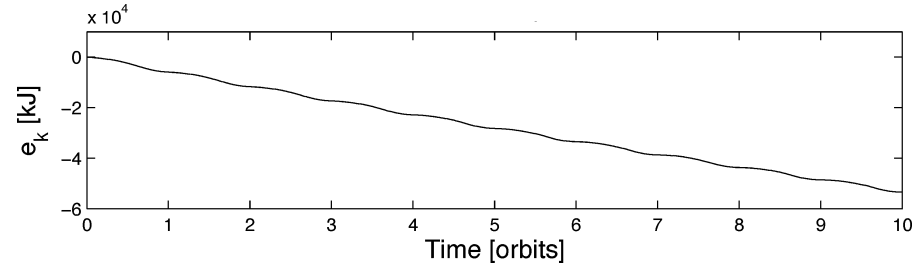


**c) Kinetic energy error**

**Fig. 5 Power, power error, kinetic energy error with damped flywheel rotors, and without kinetic energy error feedback.**

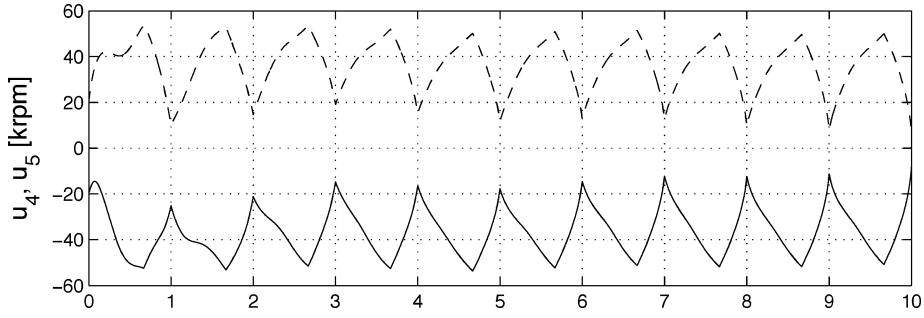


**a) Pseudoinverse**

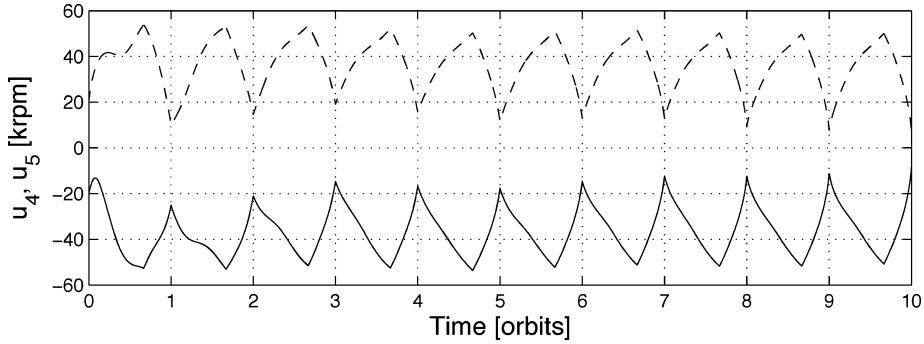


**b) Divided power**

**Fig. 6 Flywheel angular speeds with damped flywheel rotors, without kinetic energy error feedback.**

The kinetic energy error of the flywheel system is reflected in the angular speeds of the flywheels relative to $B$. Figure 6 displays the speeds of the flywheel pair whose spin axes are parallel to $\hat{\boldsymbol{b}}_1$, with $u_4$ represented by the solid curve and $u_5$ indicated by the dashed curve. Speeds of the pairs whose spin axes are parallel to $\hat{\boldsymbol{b}}_2$ and $\hat{\boldsymbol{b}}_3$ are similar, but not shown. The flywheel rotor speeds exhibit a secular decay that is most noticeable in the maxima and minima in the latter orbits. No significant difference appears between the behavior resulting from the pseudoinverse and divided power steering laws, presented in Figs. 6a and 6b, respectively.

Time histories of flywheel motor torques, in the presence of damping, are shown in Fig. 7 where the results are associated with the pseudoinverse (Fig. 7a) and divided power steering laws (Fig. 7b). A solid curve is used for $\boldsymbol{M}^{B/R_1} \cdot \hat{\boldsymbol{b}}_1$, and a dashed curve for $\boldsymbol{M}^{B/R_4} \cdot \hat{\boldsymbol{b}}_1$. The effects of damping appear to be negligible at first; however,

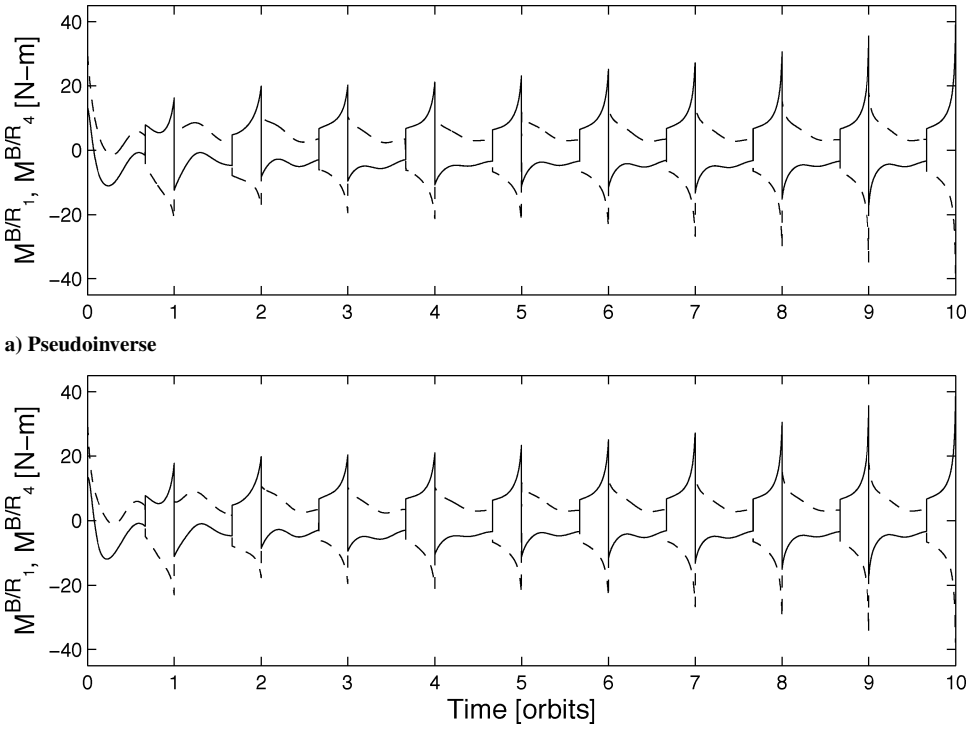


**a) Pseudoinverse**

**b) Divided power**

**Fig. 7 Flywheel motor torque with damped flywheel rotors, without kinetic energy error feedback.**

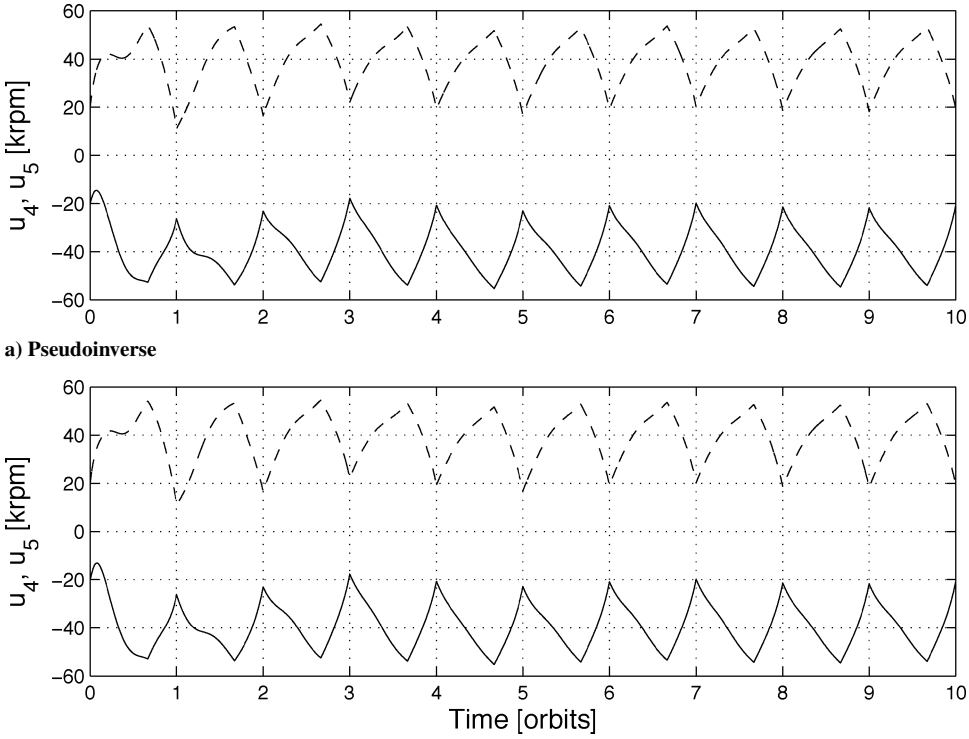


**a) Pseudoinverse**

**b) Divided power**

**Fig. 8 Flywheel angular speeds with damped flywheel rotors and kinetic energy error feedback.**

after some time it is apparent that damping causes the motor torque magnitudes to increase, with either steering law. Inspection of Eq. (48) indicates that the secular decay in rotor speeds requires an increase in motor torques to produce the required power. The increase in motor torque magnitudes implies further power losses as more electrical power must be diverted to the motor–generators to meet the attitude control and power management requirements simultaneously. Torque time histories for the other motors are quite similar to those exhibited in Fig. 7.

#### Counteracting Damping with Kinetic Energy Error Feedback

To compensate for damping, the kinetic energy error feedback design is employed with a weighting parameter $\lambda$ of 1 $s^{-2}$. The parameters of the previous simulation are used again, leading to the results shown in Figs. 8–10.

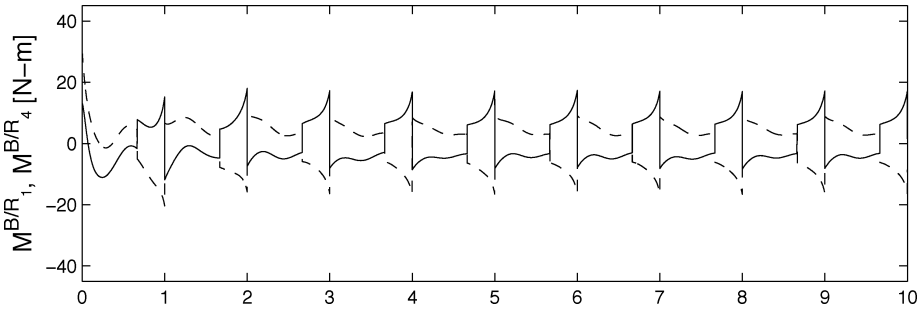


**a) Pseudoinverse**

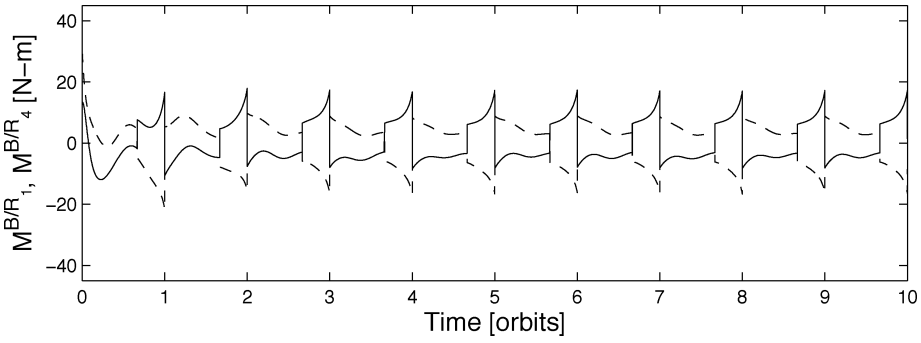


**b) Divided power**

**Fig. 9 Flywheel motor torques with damped flywheel rotors and kinetic energy error feedback.**

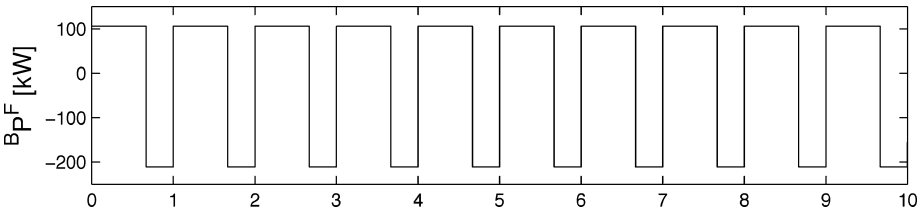


**a) Total actual power**

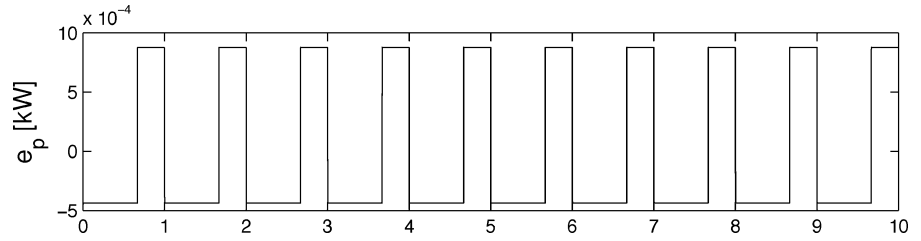


**b) Power error**

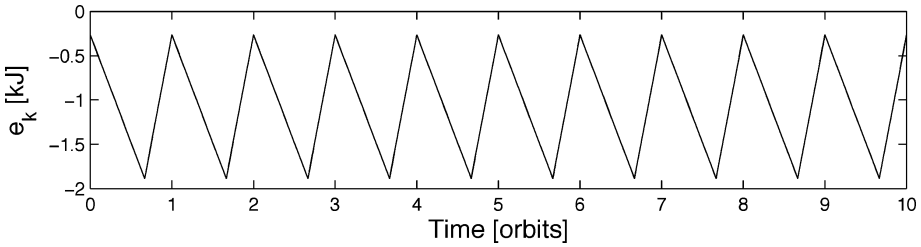


**c) Kinetic energy error**

**Fig. 10 Power, power error, and kinetic energy error with damped flywheel rotors, and kinetic energy error feedback.**

As explained in Ref. 4, the planned speed range for the FESS rotors was 60,000–18,000 rpm. This speed range of approximately 3–1, typical of current flywheel designs, corresponds to a depth of discharge of 91%. Figure 8 shows that the rotor speeds remain within the intended range and that kinetic energy feedback eliminates the secular decay of rotor speeds seen to result from flywheel rotor damping in Fig. 6. The flywheel motor torques are shown in Fig. 9. It is immediately clear that the magnitudes do not increase with time as they do in Fig. 7. The power error $e_p$ shown in Fig. 10b is quite small and leads to the kinetic energy error $e_k$ shown in Fig. 10c. It is small and periodic, in contrast to the secular decay obtained without energy feedback ($\lambda = 0\ \mathrm{s}^{-2}$).

The kinetic energy error feedback method compensates for damping very effectively, as shown by Figs. 8–10; these results are virtually the same as those obtained with $C_d = 0$ and no energy

feedback, although space limitations prevent us from including them separately.

**Comparison of Steering Laws**

In the results presented thus far, two steering laws have been used to determine the flywheel motor torques necessary to meet the attitude control and power management requirements simultaneously. The first of these involves formation of a pseudoinverse to solve an underdetermined system of equations for flywheel motor torques, whereas the second divides the power requirements evenly among the three pairs of rotors, resulting in a uniquely determined solution. The objective of both approaches is to produce the same control torque $\bar{\tau}$ and required power ${}^{B}\bar{P}^{F}$; therefore, it is not surprising that large differences are not discernible in Figs. 6a–9a and 6b–9b. A more detailed comparison of the differences is now undertaken with the aid of Figs. 11 and 12, where results obtained with

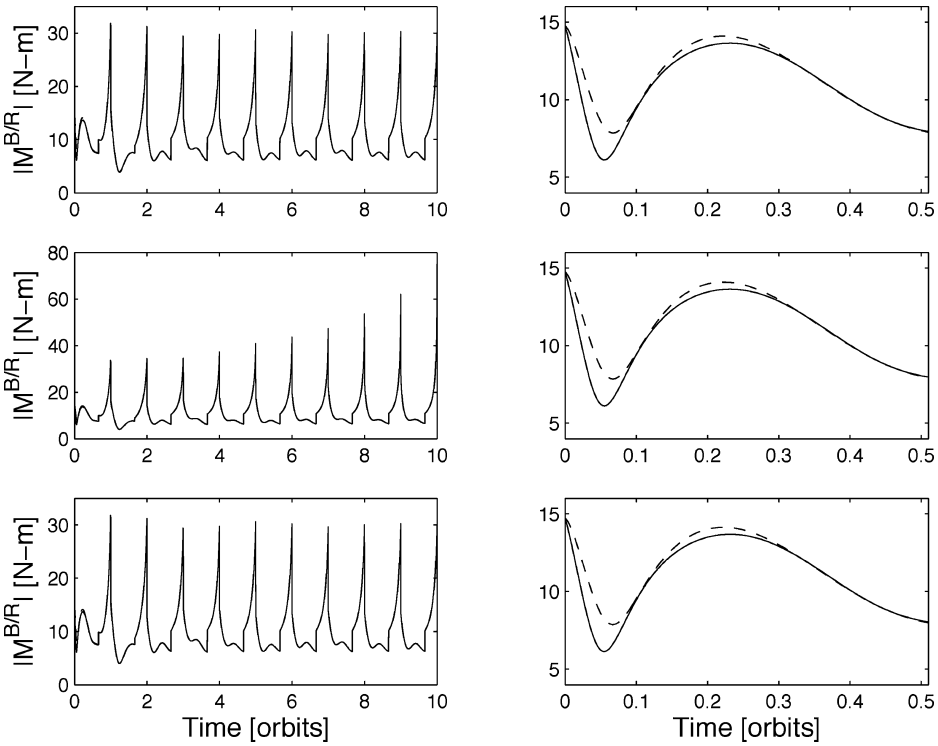


**a) Magnitude of motor torque** **b) Magnitude of motor torque (detail)**

**Fig. 11 Root sum square of flywheel motor torques with no damping, damping without kinetic energy error feedback, and damping with feedback.**

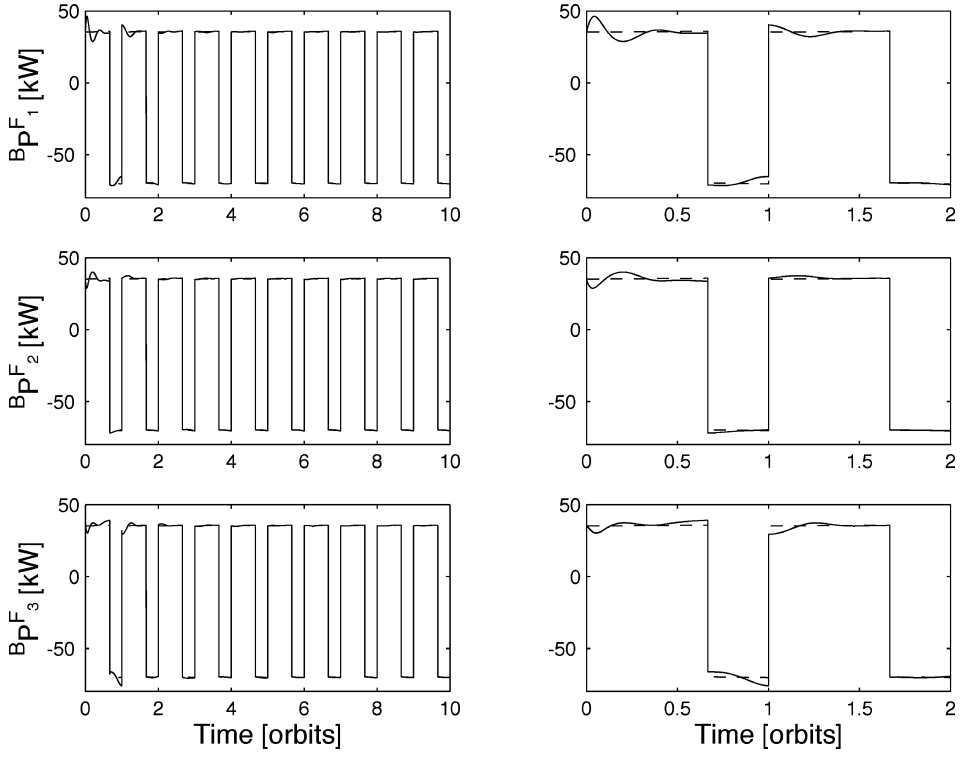


**a) Power distribution** **b) Power distribution (detail)**

**Fig. 12 Power distribution in each axis with damped flywheel rotors, with kinetic energy error feedback.**

the pseudoinverse and divided power methods are displayed with solid and dashed lines, respectively.

Figure 11 shows time histories of the square root of the sum of the squares of the motor torques,

$$\left\{ \sum_{i=1}^{3} \left[ \left( \boldsymbol{M}^{B/R_i} \cdot \hat{\boldsymbol{b}}_i \right)^2 + \left( \boldsymbol{M}^{B/R_{i+3}} \cdot \hat{\boldsymbol{b}}_i \right)^2 \right] \right\}^{\frac{1}{2}}$$

a quantity that is minimized by the pseudoinverse approach. Curves associated with undamped flywheel rotors are contained in the first row, damped rotors in the second row, and damped rotors with kinetic energy error feedback in the third row. The solutions of the pseudoinverse and divided power methods are indistinguishable from one another when viewed over an interval of 10 orbits in Fig. 11a; consequently, detailed plots are shown in Fig. 11b for the first-half of an orbit. As expected, it can be seen that the minimum-norm solution of the pseudoinverse method is always less than or equal to the result given by the divided-power method. Figures 11 also seem to indicate that the pseudoinverse solution approaches the divided-power solution in the steady state. The benefit of the kinetic energy error feedback is apparent once more, by comparing the growth in the second row of Fig. 11a with the absence of growth in the third row.

Figure 12 shows the distribution of power among the flywheel pairs when damping is ameliorated by feedback of kinetic energy error. The first row contains the power ${}^{B}P^{F_1}$ [see Eqs. (58)] of the rotor pair whose spin axes are aligned with $\hat{\boldsymbol{b}}_1$, and the second and third rows show ${}^{B}P^{F_2}$ and ${}^{B}P^{F_3}$. A detail of Fig. 12a for the first two orbits is shown in Fig. 12b.

Naturally, the divided-power steering law distributes the power and energy equally between the three flywheel pairs. The pseudoinverse steering law apportions the power profile among the three pairs in such a way that the total power requirement is met, but the minimum-norm solution for motor torques yields an unequal distribution of power and energy in the initial orbits. As noted in connection with Fig. 11, the power distribution resulting from the pseudoinverse steering law appears to approach that of the divided power law in the steady state. The conclusion to be drawn from Figs. 11 and 12 is that the pseudoinverse steering law accomplishes minimization of the square root of the sum of the squares of the motor torques by distributing the power equally in all three orthogonal axes in the steady state, that is, in the state of TEA.

## Conclusions

General, nonlinear equations governing motion of a rigid spacecraft containing flywheels and CMGs are presented in vector-dyadic form. A set of 12 scalar equations is obtained by applying the generic relationships to the special case of a complex gyrostat with 3 pairs of flywheels mounted in orthogonal directions. Existing literature contains equations for describing motion of a spacecraft with CMGs; they follow from the generic ones under two reasonable assumptions. The exact equations for the complex gyrostat and the approximate relationships associated with CMGs are combined to form approximate equations for a spacecraft with flywheels and CMGs and are subsequently linearized and nondimensionalized in preparation for design of linear control laws.

A control law has been designed for an Earth-pointing spacecraft, and numerical simulation shows that it performs well in controlling torque equilibrium attitude, the energy stored in counter-rotating flywheels, and angular momentum of the flywheels and CMGs. Two steering laws are developed for ensuring that attitude control and energy storage requirements are met simultaneously by the flywheels. The design of a method for feeding back error in the rotational kinetic energy of the flywheel rotors to eliminate problems caused by rotor damping is shown to be effective.

One topic of future research that may be valuable is the study of controller performance in the face of imperfect knowledge of spacecraft inertia properties, or flywheel rotor pairs whose axial moments of inertia are not identical. Inclusion of a prefilter would allow the control laws to estimate these parameters from attitude response and to compensate for any significant changes in the mass distribution of the spacecraft over time. Another topic with possible merit is exploration of the best way to apportion the control torque between the flywheels and CMGs; an adaptive feature for distributing the workload unequally could be preferable to the practice of sharing it equally. Future spacecraft are likely to rely solely on flywheels, rather than a mixture of flywheels and CMGs, and the control laws developed here are easily applied to this special case.

The promising simulation results demonstrated here for control of power, momentum, and attitude of Earth-pointing spacecraft suggest that it would be worthwhile to examine the very important class of inertially oriented spacecraft.

## Acknowledgments

The research described herein was conducted as part of the NASA Langley Research Center Creativity and Innovation initiative, and the authors are sincerely appreciative of all the support we received. A more detailed report of this work, which includes additional control law designs and simulation results, is available in Roithmayr, C. M., Karlgaard, C. D., Kumar, R. R., Seywald, H., and Bose, D. M., "Dynamics and Control of Attitude, Power, and Momentum for a Spacecraft Using Flywheels and Control Moment Gyroscopes," NASA TP-2003-212178, April 2003. The first author is especially grateful to the management of the Aerospace Systems Concepts and Analysis Competency and the Spacecraft and Sensors Branch for their encouragement.

## References

[1]Christopher, D. A., and Beach, R., "Flywheel Technology Development Program for Aerospace Applications," *IEEE Aerospace and Electronic Systems Magazine*, Vol. 13, No. 6, 1998, pp. 9–14.

[2]Van Tassel, K. E., and Simon, W. E., "Inertial Energy Storage for Advanced Space Station Applications," *Proceedings of the 20th Intersociety Energy Conversion Engineering Conference*, Society of Automotive Engineers, Warrendale, PA, Vol. 2, 1985, pp. 337–342.

[3]Oglevie, R. E., "Wheel Configurations for Combined Energy Storage and Attitude Control Systems," AIAA Paper 85-1989, Aug. 1985.

[4]Roithmayr, C. M., "International Space Station Attitude Motion Associated With Flywheel Energy Storage," *Proceedings of the Space Technology and Applications International Forum*, American Institute of Physics, Melville, NY, Feb. 2000, pp. 454–459.

[5]Wie, B., Byun, K. W., Warren, V. W., Geller, D., Long, D., and Sunkel, J., "New Approach to Attitude/Momentum Control for the Space Station," *Journal of Guidance, Control, and Dynamics*, Vol. 12, No. 5, 1989, pp. 714–722.

[6]Harduvel, J. T., "Continuous Momentum Management of Earth-Oriented Spacecraft," *Journal of Guidance, Control, and Dynamics*, Vol. 15, No. 6, 1992, pp. 1417–1426.

[7]Kennel, H. F., "Steering Law for Parallel Mounted Double-Gimbaled Control Moment Gyros—Revision A," NASA TM-82390, Marshall Space Flight Center, Huntsville, AL, Jan. 1981.

[8]Notti, J. E., Cormack, A., and Klein, W. J., "Integrated Power/Attitude Control System (IPACS)," AIAA Paper 74-921, Aug. 1974.

[9]Will, R. W., Keckler, C. R., and Jacobs, K. L., "Description and Simulation of an Integrated Power and Attitude Control System Concept for Space-Vehicle Application," NASA TN D-7459, Langley Research Center, Hampton, VA, April 1974.

[10]Hall, C. D., "High Speed Flywheels for Integrated Energy Storage and Attitude Control," *Proceedings of the 1997 American Control Conference*, Vol. 3, American Automatic Control Council, Evanston, IL, 1997, pp. 1894–1898.

[11]Tsiotras, P., Shen, H., and Hall, C. D., "Satellite Attitude Control and Power Tracking with Energy/Momentum Wheels," *Journal of Guidance, Control, and Dynamics*, Vol. 24, No. 1, 2001, pp. 23–34.

[12]Costic, B. T., de Queiroz, M. S., Dawson, D. M., and Fang, Y., "Energy Management and Attitude Control Strategies using Flywheels," *Proceedings of the 40th IEEE Conference on Decision and Control*, Inst. of Electrical and Electronics Engineers, Piscataway, NJ, 2001, pp. 3435–3440.

[13]Fausz, J. L., and Richie, D. J., "Flywheel Simultaneous Attitude Control and Energy Storage Using a VSCMG Configuration," *Proceedings of the 2000 IEEE International Conference on Control Applications*, Inst. of Electrical and Electronics Engineers, Piscataway, NJ, 2000, pp. 991–995.

[14]Richie, D. J., Tsiotras, P., and Fausz, J. L., "Simultaneous Attitude Control and Energy Storage Using VSCMGs—Theory and Simulation," *Proceedings of the 2001 American Control Conference*, Vol. 5, Inst. of Electrical and Electronics Engineers, Piscataway, NJ, 2001, pp. 3973–3979.

[15]Yoon, H., and Tsiotras, P., "Spacecraft Adaptive Attitude and Power Tracking with Variable Speed Control Moment Gyroscopes," *Journal of Guidance, Control, and Dynamics*, Vol. 25, No. 6, 2002, pp. 1081–1090.
[16]Varatharajoo, R., and Fasoulas, S., "Methodology for the Development of Combined Energy and Attitude Control Systems for Satellites," *Aerospace Science and Technology*, Vol. 6, No. 4, 2002, pp. 303–311.
[17]Kascak, P. E., Jansen, R. H., Kenny, B., and Dever T. P., "Single Axis Attitude Control and DC Bus Regulation With Two Flywheels," NASA TM-2002-211812, John H. Glenn Research Center, Cleveland, OH, Aug. 2002.
[18]Kenny, B. H., and Kascak, P. E., "DC Bus Regulation With a Flywheel Energy Storage System," NASA TM-2002-211897/REV1, John H. Glenn Research Center, Cleveland, OH, Jan. 2003.
[19]Kenny, B. H., Kascak, P. E., Jansen, R., and Dever T., "A Flywheel Energy Storage System Demonstration for Space Applications," NASA TM-2003-212346, John H. Glenn Research Center, Cleveland, OH, June 2003.
[20]Kane, T. R., and Levinson, D. A., *Dynamics: Theory and Applications*, McGraw–Hill, New York, 1985, pp. 106, 124, 125, 159.
[21]Mitiguy, P. C., and Reckdahl, K. J., "Efficient Dynamical Equations for Gyrostats," *Journal of Guidance, Control, and Dynamics*, Vol. 24, No. 6, 2001, pp. 1144–1156.
[22]Rheinfurth, M. H., and Carroll, S. N., "Space Station Rotational Equations of Motion," NASA TP 2511, Marshall Space Flight Center, Huntsville, AL, 1985.
[23]Kane, T. R., Likins, P. W., and Levinson, D. A., *Spacecraft Dynamics*, McGraw–Hill, New York, 1983, pp. 113, 211, 221, 423.
[24]Bryson, A. E., and Ho, Y.-C., *Applied Optimal Control*, Hemisphere, New York, 1975, p. 149.
[25]Roithmayr, C. M., "International Space Station Attitude Control and Energy Storage Experiment: Effects of Flywheel Torque," NASA TM-1999-209100, Langley Research Center, Hampton, VA, Feb. 1999.
[26]Lay, D. C., *Linear Algebra and its Applications*, Addison–Wesley, Reading, MA, 1994, pp. 433, 434.
[27]Goodzeit, N. E., Paluszek, M. A., and Cohen, W. J., "Attitude Control System with Reaction Wheel Friction Compensation," U.S. Patent 5,201,833, filed 13 April 1993.